Brain-Derived Neurotrophic Factor Induces Sustained Elevation of Intracellular Ca^{2+} in Rodent Microglia[1]

Yoshito Mizoguchi,* Akira Monji,[2]* Takahiro Kato,* Yoshihiro Seki,*† Leo Gotoh,* Hideki Horikawa,* Satoshi O. Suzuki,† Toru Iwaki,† Miyuki Yonaha,* Sadayuki Hashioka,* and Shigenobu Kanba*

Microglia are intrinsic immune cells that release factors, including proinflammatory cytokines, NO, and neurotrophins, following activation after disturbance in the brain. Elevation of intracellular Ca^{2+} concentration ($[Ca^{2+}]i$) is important for microglial functions, such as the release of cytokines and NO from activated microglia. There is increasing evidence suggesting that pathophysiology of neuropsychiatric disorders is related to the inflammatory responses mediated by microglia. Brain-derived neurotrophic factor (BDNF) is a neurotrophin well known for its roles in the activation of microglia as well as in pathophysiology and/or treatment of neuropsychiatric disorders. In this study, we observed that BDNF induced a sustained increase in $[Ca^{2+}]i$ through binding with the truncated tropomyosin-related kinase B receptor, resulting in activation of the PLC pathway and store-operated calcium entry in rodent microglial cells. RT-PCR and immunocytochemical techniques revealed that truncated tropomyosin-related kinase B-T1 receptors were highly expressed in rodent microglial cells. Sustained activation of store-operated calcium entry occurred after brief BDNF application and contributed to the maintenance of sustained $[Ca^{2+}]i$ elevation. Pretreatment with BDNF significantly suppressed the release of NO from activated microglia. Additionally, pretreatment of BDNF suppressed the IFN-γ-induced increase in $[Ca^{2+}]i$, along with a rise in basal levels of $[Ca^{2+}]i$ in rodent microglial cells. We show direct evidence that rodent microglial cells are able to respond to BDNF, which may be important for the regulation of inflammatory responses, and may also be involved in the pathophysiology and/or the treatment of neuropsychiatric disorders. ***The Journal of Immunology,*** **2009, 183: 7778–7786.**

Microglia are the intrinsic immune cells which release many factors, including proinflammatory cytokines, NO and neurotrophic factors, when they are activated in response to brain injury or immunological stimuli (1, 2). Recent in vivo imaging has shown that microglial cells are highly active with motile protrusions even in their resting state (3). There is increasing evidence suggesting that pathophysiology of neuropsychiatric disorders, such as schizophrenia (4) or depression (5, 6), is related to the inflammatory responses mediated by microglial cells. We have recently reported that pretreatment with antidepressants (7) or antipsychotics (8, 9) significantly inhibited the release of NO and cytokines from activated microglia, respectively. These reports indicated that agents that are able to inhibit microglial activation could be useful for the treatment of neuropsychiatric disorders.

Brain-derived neurotrophic factor (BDNF)[3] has various important roles in cell survival, apoptosis, gene expression, neurite outgrowth, cellular morphology, synaptic plasticity, and neurotransmitter release in the CNS (10–14). In the rodent brain, microglial cells express BDNF mRNA (15) and secrete BDNF following stimulation with LPS (16). BDNF released from activated microglia then induces the sprouting of nigrostriatal dopaminergic neurons (17), causing a shift in the neuronal anion gradient (18), or promotes the proliferation and survival of microglia themselves (15, 19). To date, BDNF is also well known for its involvement in the pathophysiology of neuropsychiatric disorders (20–24).

In the CNS, intracellular Ca^{2+} signaling regulates many different cellular functions, such as cell proliferation, gene transcription or exocytosis at synapses (25). Elevation of intracellular Ca^{2+} is important in activation of microglial cell functions, including proliferation, release of NO and cytokines, migration, ramification, and deramification (26, 27). Recently, Trang et al. (28) showed that influx of extracellular Ca^{2+} causes the release of BDNF from microglial cells and it has been shown that alteration of intracellular Ca^{2+} signaling underlies the pathophysiology of neuropsychiatric disorders, including schizophrenia (29), depression, and bipolar disorder (30).

BDNF is known to induce a rapid increase in intracellular Ca^{2+} in neurons (13, 31, 32) and in astrocytes (33). However, there have been no prior reports on how BDNF affects intracellular Ca^{2+} mobilization in microglial cells. In this study, we examined whether BDNF affects intracellular Ca^{2+} signaling in rodent microglial cells, using fura-2 imaging.

*Department of Neuropsychiatry, Graduate School of Medical Science, Kyushu University, Fukuoka, Japan; and †Department of Neuropathology, Neurological Institute, Graduate School of Medical Sciences, Kyushu University, Fukuoka, Japan

Received for publication April 27, 2009. Accepted for publication October 6, 2009.

The costs of publication of this article were defrayed in part by the payment of page charges. This article must therefore be hereby marked *advertisement* in accordance with 18 U.S.C. Section 1734 solely to indicate this fact.

[1] This work was supported by research grants from the Ministry of Education, Culture, Sports, Science and Technology, Japan (to Y.M., A.M., and S.K.) and the Ministry of Health, Labour and Welfare, Japan (to S.K.). T.K. is a research fellow of the Japan Society for the Promotion of Science, and is supported by Mitsubishi Pharma Research Foundation.

[2] Address correspondence and reprint requests to Akira Monji, Department of Neuropsychiatry, Graduate School of Medical Sciences, Kyushu University, 3-1-1 Maidashi Higashi-ku, Fukuoka, Japan. E-mail address: amonji@hf.rim.or.jp

[3] Abbreviations used in this paper: BDNF, brain-derived neurotrophic factor; 2-APB, 2-aminoethyl diphenylborinate; NGF, nerve growth factor; NT-3, neurotrophin-3; TrkB, tropomyosin-related kinase B; NB, neurobasal medium; TrkB-FL, full-length form of TrkB; PLC, phospholipase C; IP_3, inositol trisphosphate; SOCE, store-operated calcium entry; TRP channel, transient receptor potential channel.

www.jimmunol.org/cgi/doi/10.4049/jimmunol.0901326

Materials and Methods

Materials

The drugs used in the present study include ATP, U73122, U73343, LY294002, thapsigargin, 2-aminoethyl diphenylborinate (2-APB), SKF-96365, nerve growth factor (NGF), neurotrophin-3 (NT-3) (all from Sigma-Aldrich), K252a (Calbiochem) and polyclonal rabbit anti-tropomyosin-related kinase B (TrkB) receptor Ab (ab33655; Abcam). Drugs that were insoluble in water were first dissolved in DMSO and then diluted in the standard external solution. The final concentration of DMSO was always <0.1%. Recombinant IFN-γ and mouse GM-CSF were purchased from R&D Systems. Human recombinant BDNF (Sigma-Aldrich) was diluted with the standard external solution to obtain the final concentration (20 ng/ml; 0.73 nM). This BDNF concentration is sufficient to promote the proliferation of microglial cells (15) or to rapidly elevate $[Ca^{2+}]i$ in astrocytes (33) and also in neurons (12, 31).

Primary microglial cells

Primary microglial cells were prepared as described previously (9). Primary mixed cells were prepared from the whole brain of 3-day postnatal Sprague-Dawley (SD) rats using a Cell Strainer (BD Falcon). Primary rat microglial cells were selected after attachment to Aclar film (Nisshin EM) for 2 h in DMEM supplemented with 10% FBS (10% FBS/DMEM). Aclar films were gently washed with PBS, then transferred to fresh 10% FBS/DMEM, and the fresh microglia expanded for 1–2 days. The purity of isolated microglia was assessed by immunocytochemical staining for the microglial marker, Iba-1, and >99% of cells stained positively.

The 6-3 microglial cells

The murine microglial cell line, 6-3, was donated by Dr. Makoto Sawada of Nagoya University (Japan). The 6-3 cells were established from neonatal C57BL/6J (H-2b) mice using a nonenzymatic and nonvirus-transformed procedure (8, 9, 34). The 6-3 cells were cultured in Eagle's MEM supplemented with 0.3% $NaHCO_3$, 2 mM glutamine, 0.2% glucose, 10 g/ml insulin, and 10% FCS. Cells were maintained at 37°C in a 10% CO_2, 90% air atmosphere. GM-CSF was supplemented into the culture medium, at a final concentration of 1 ng/ml, to maintain proliferation of the 6-3 cells (34). Culture medium was renewed twice per week. The 6-3 cells are shown to closely resemble primary microglial cells (9).

Cultured neurons and astrocytes

To obtain pure neuronal cultures, the dissected tissues were prepared from the hippocampus of 15-day-embryonic SD rats. The dissected tissues were dissociated with a cell strainer and suspended in neurobasal medium (NB) supplemented with B27, L-glutamine, penicillin/streptomycin/amphotericin B (all from Life Technologies), EGF, basic FGF (both from Sigma-Aldrich), and was referred to as NB/B27/L-glutamine/EGF/FGF/PSA. Cells were plated at a density of 2×10^6 cells/well in 6-well plates and incubated at 37°C in an incubator with a 5% CO_2 in air atmosphere. Seven days after plating, the cultured cells were dissociated by trypsinization and microglia removed by adhesion to the Aclar plastic film for 2 h in NB/B27/L-glutamine/EGF/FGF/PSA. Following removal of microglial cells, the cultured cells were subsequently maintained in Neurobasal-A medium supplemented with B27-A (both from Life Technologies), L-glutamine, basic FGF, and PSA for 5 days. Cultured astrocytes were prepared from the subventricular zone of the forebrain of 3-day postnatal SD rats using a Cell Strainer. The dissociated cells were incubated in 10% FBS/DMEM. Seven days after plating, most cells were glial fibrillary acidic protein-immunopositive astrocytes.

Intracellular Ca^{2+} imaging

The experiments were performed as reported previously (9, 31). The intracellular Ca^{2+} concentration ($[Ca^{2+}]i$) in response to BDNF was monitored using fura-2 AM (acetoxymethyl ester; Ref. 35) in both 6-3 and primary microglial cells. The experiments were performed in the external standard solution (in mM: 150 NaCl, 5 KCl, 2 $CaCl_2$, 1 $MgCl_2$, 10 glucose and 10 HEPES (pH 7.4) with Tris-OH) (12–14, 31) at room temperature (25°C). The Ca^{2+}-free external solution was obtained by adding EGTA (2 mM) and removing $CaCl_2$ from the external standard solution. Aluminum fluoride (AlF_4^-) solution contained (in mM: 120 KCl, 10 NaCl, 10 NaF, 0.03 $AlCl_3$, 1 EGTA, 0.5 $CaCl_2$, 2 $MgCl_2$ and 10 HEPES (pH 7.4) with Tris-OH).

The 6-3 or primary microglial cells plated on a glass-base dish (Iwaki) were loaded with 5 μM fura-2 AM (Dojindo) for 20 min and washed three times with the external standard solution before measurement. During measurement, using an Olympus IX70–22FL inverted microscope and a ×20 objective (Olympus), the external standard solution was constantly perfused (10 ml/min). For fura-2 excitation the cells were illuminated with two alternating wavelengths, 340 and 380 nm using a computerized system for a rapid dual wavelength Xenon arc. The emitted light was recorded at 510 nm using a cooled CCD camera (C4742–95ER; Hamamatsu Photonics) and images were saved every 5 or 10 s. These series of sequential data were analyzed using the AquaCosmos software package (Hamamatsu Photonics). The $[Ca^{2+}]i$ was calculated from the ratio (R) of fluorescence recorded at 340 and 380 nm excitation wavelengths for each pixel within a microglial cell boundary. Calibrations (conversion of R340/380 values into calcium concentrations) were performed as described previously (9, 35), using a fura-2 calcium imaging calibration kit (Molecular Probes). Basal $[Ca^{2+}]i$ was determined from the initial 12 images of each cell recording. A $[Ca^{2+}]i$ signal was defined as an increase in R 340/380 with clear time correlation to the application of BDNF. Increase of $[Ca^{2+}]i$ in response to BDNF was calculated as the difference between basal $[Ca^{2+}]i$ and values obtained at 15 min after a 3 min treatment of BDNF. All data presented were obtained from at least five dishes and three different cell preparations. Data are expressed as the mean ± SEM and statistical comparisons were made using an unpaired *t* test.

Immunocytochemistry

Rodent microglial cells were maintained on Aclar films as described previously (9). After being rinsed twice in 0.1 M HEPES/KOH, cells were fixed with 4% paraformaldehyde for 10 min, and then rinsed with 0.1M HEPES/KOH for 10 min. Indirect immunofluorescence was performed using the following Abs; polyclonal rabbit anti-TrkB receptor Ab which recognizes truncated forms of mouse TrkB receptor (1/500 dilution; Santa Cruz Biotechnology) and mouse anti-CD45 mAb (1/100 dilution; Serotec). These specimens were incubated in primary Abs diluted in 0.1% Triton X-100 in PBS containing 5% normal goat serum at 4°C overnight. After being rinsed twice with PBS for 5 min, FITC- or Texas red-conjugated secondary Abs (Southern Biotechnology Associates) were used for detection.

RT-PCR

Total RNA was isolated from rat primary microglial cells, murine 6-3 microglial cells, rat cultured neurons, or rat cultured astrocytes using the RNeasy Mini Kit (Qiagen). RT-PCR was performed with reagents included in the SuperScript III RT-PCR System (Invitrogen), RNA and gene-specific primers for β-actin (forward: 5′-TAAAACGCAGCTCAGTAACA GTCCG-3′ and reverse: 5′-TGGAATCCTGTGGCATCCATGAAAC-3′), TrkB-T1 receptor (forward: 5′-CGGGAGCATCTCTCGGTCT-3′ and reverse: 5′-AGGGGGATCTTATGAAACAAA-3′) and full-length form of TrkB (TrkB-FL) receptor (forward: 5′-ATGCTGCACATCGCTCAGCA-3′ and reverse: 5′-ATGGGCAACATTGTGTGGCC-3′) as previously described (33). Reverse transcription and amplification was conducted in a gradient cycler (Biometra). The reaction mixture was incubated at 94°C for 2 min to fully activate the *Taq*DNA polymerase, followed by a touchdown protocol with denaturing at 94°C for 15 s, annealing from 94 to 60°C for 30 s, and extension at 68°C for 30 s over 40 cycles. Finally, a 5 min extension at 68°C was conducted. PCR products were resolved by electrophoresis in 2% agarose gels stained with ethidium bromide, and photographed. The predicted size was checked against a 100 bp DNA ladder (Biobeer).

NO release assessment

The 6-3 microglial cells were plated on 96-well tissue culture plates at 1×10^5 cells per 200 μl per well and then were preincubated in the presence or absence of BDNF for 12 h and then incubated in the presence or absence of 50 U/ml IFN-γ at 37°C. After 48 h, the collected medium was assayed for NO accumulation. NO released into the culture medium was measured using a Griess reaction assay kit (Dojindo). The absorbance of the Griess reaction was read at 540 nm using a plate reader (Labsystems Multiscan).

Cell viability

Cell viability was determined by colorimetric measurements of the reduction product of 3-[4,5-dimethylthiazol-2-yl]-2,5-diphenyltetrazolium bromide (MTT). After treatment with or without BDNF, the original medium was removed from the 96-well plates and the cells incubated for 2 h at 37°C in the presence of phenol red-free MEM (Invitrogen) containing 0.5 mg/ml MTT. A 100 μl MTT lysis buffer (5% sodium dodecylsulfate and 5 mM HCl) was added to each well and the plates incubated at 37°C overnight to dissolve the formazan that had formed in the wells. MTT is reduced to formazan in the mitochondria of living cells. Reduced MTT was measured by means of a plate reader at a wavelength of 570 nm.

Statistics

All data are represented as the means ± SEM and they were analyzed by a one-way ANOVA followed by Turkey's PLSD post hoc test for specific comparisons. Significance was established at a level of $p < 0.05$.

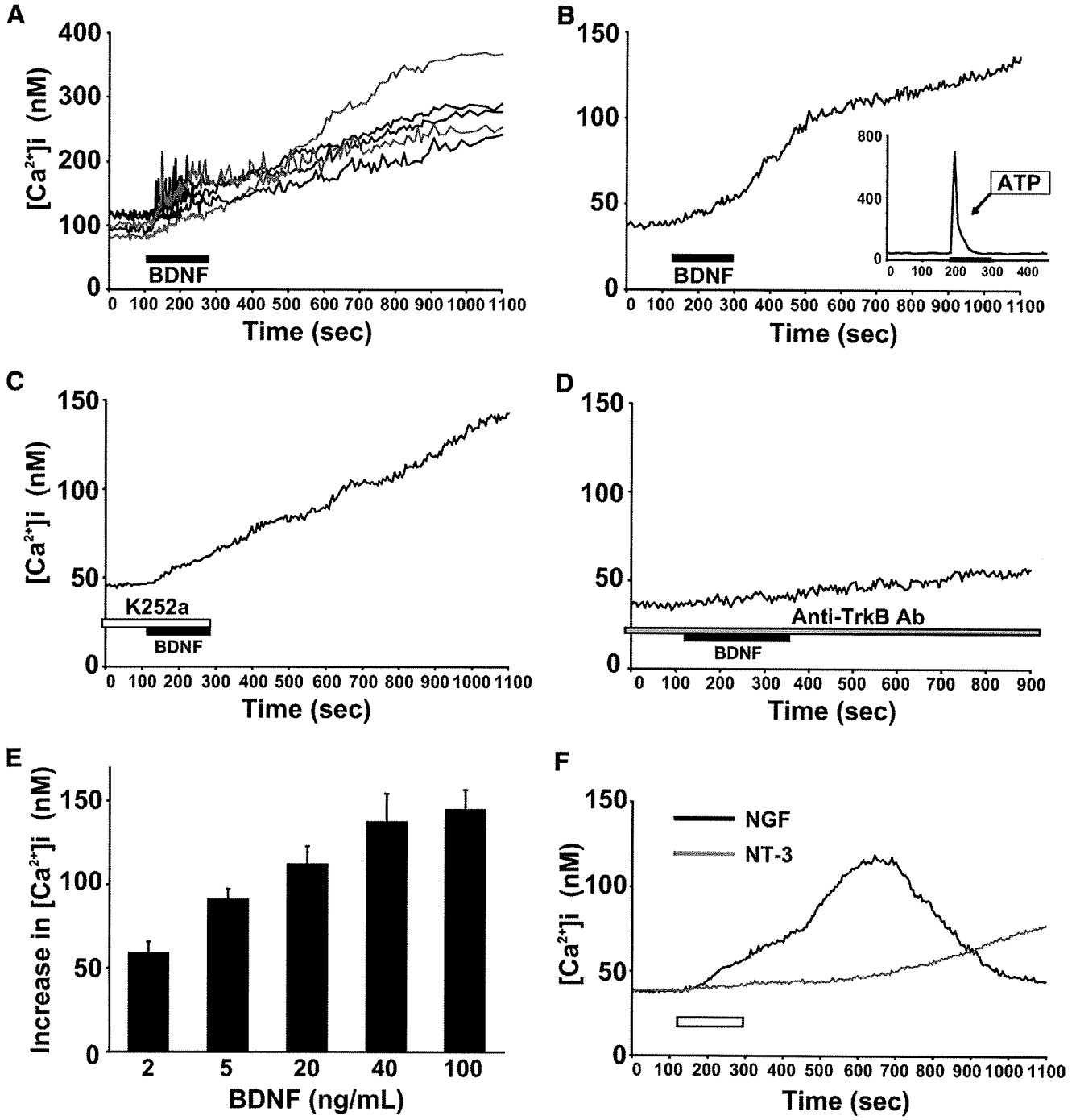

FIGURE 1. BDNF induces sustained elevation of intracellular Ca^{2+} through binding to the truncated TrkB receptors. *A*, Five representative traces showing a brief (3 min) treatment of 20 ng/ml BDNF-induced sustained increase in $[Ca^{2+}]i$ in murine 6-3 microglial cells. *B*, A brief (3 min) treatment of 20 ng/ml BDNF-induced sustained increase in $[Ca^{2+}]i$ in primary rat microglial cells. The *inset* shows a 100 μM ATP-induced transient increase in $[Ca^{2+}]i$ in primary rat microglial cells. The average trace of 10 $[Ca^{2+}]i$ traces in response to ATP is shown. *C*, BDNF induced a sustained increase in $[Ca^{2+}]_i$ when K252a (200 nM), a membrane-permeant inhibitor of TrkB receptor tyrosine kinase, was present in primary rat microglial cells. *D*, When anti-TrkB Ab, which recognizes the entire extracellular domain of TrkB receptors, was present BDNF did not elevate $[Ca^{2+}]i$ in primary rat microglial cells. *E*, The dose-response effect of different concentrations of BDNF on the amplitude of $[Ca^{2+}]i$ increase obtained 15 min after BDNF treatment in primary rat microglial cells (values are the mean plus SE). *F*, Average traces demonstrating the effect of 20 ng/ml NGF (black line) or 20 ng/ml NT-3 (gray line) on intracellular Ca^{2+} mobilization in primary rat microglial cells. In *B*, *C*, *D*, and *F* each panel shows the average trace resulting from five representative traces of $[Ca^{2+}]i$ in each condition.

Results

BDNF induces sustained elevation of intracellular Ca^{2+} through the binding to truncated neurotrophin TrkB receptors in rodent microglial cells

We first tested the effect of BDNF on intracellular Ca^{2+} mobilization in rodent microglial cells, using fura-2 imaging. A brief (3 min) application of BDNF (20 ng/ml) induced a sustained elevation of intracellular Ca^{2+} in both 6-3 (n = 195; Fig. 1*A*) and primary (n = 73; Fig. 1*B*) microglial cells tested. In every cell, the time to onset was constantly within 30 s after the start of BDNF application. Once the intracellular Ca^{2+} rose, it gradually increased and reached a steady state level without attenuation. The

increase in intracellular Ca^{2+} was sustained for >40 min even after the washout of BDNF until the end of recording. In primary microglial cells, BDNF elevated $[Ca^{2+}]i$ in a dose-dependent manner (Fig. 1*E*).

In contrast, a brief (2 min) application of 100 μM ATP rapidly induced a transient intracellular Ca^{2+} elevation in both 6-3 (n = 1256) and primary (n = 121) microglial cells. In primary microglial cells, the mean amplitude of increase in $[Ca^{2+}]i$ induced by 100 μM ATP was 621.8 ± 50.2 nM (n = 121), and this value as well as the shape of response to ATP were similar to those previously reported in cultured human microglial cells (36).

BDNF binds to TrkB, a neurotrophin receptor, and there are three TrkB receptor isoforms in the mammalian brain. The TrkB-FL receptor contains a catalytic domain of tyrosine kinase which activates intracellular signaling (37). Two truncated forms of TrkB (TrkB-T1 and TrkB-T2) receptors possess the same extracellular domain, transmembrane domain and the first 12 intracellular amino acid sequences as the TrkB-FL receptor, while they lack tyrosine kinase activity (38).

We next examined the involvement of TrkB receptor tyrosine kinase activity in the BDNF-induced sustained elevation of intracellular Ca^{2+}. In the presence of K252a (200 nM), a membrane-permeable inhibitor of Trk receptor tyrosine kinase (39), BDNF (20 ng/ml) induced a sustained elevation of intracellular Ca^{2+} in both 6–3 (n = 35; Fig. 3*C*) and primary microglial cells (n = 34; Fig. 1*C*). K252a (200 nM) did not affect the base-line level of $[Ca^{2+}]i$ (Fig. 1*C*). K252a has been shown to completely block the TrkB-FL receptor-mediated signaling in some neurons (12–14, 31, 40, 41). Thus, these results suggest that the BDNF-induced sustained elevation of intracellular Ca^{2+} did not require the activation of TrkB receptor tyrosine kinases.

Previous reports clearly show that pretreatment with anti-TrkB receptor Ab can block the binding of BDNF to TrkB receptors and prevent the activation of intracellular signaling pathways (42, 43). In the presence of anti-TrkB Ab (1 μg/ml), which recognizes the entire extracellular domain corresponding to residues 1–429 (44) of rat TrkB receptor, BDNF did not elevate $[Ca^{2+}]i$ in both 6–3 (n = 67; Fig. 3*C*) or primary microglial cells (n = 56; Fig. 1*D*). Anti-TrkB Ab by itself did not affect the base-line level of $[Ca^{2+}]i$. Together, these results suggest that BDNF induced a sustained elevation of intracellular Ca^{2+} through binding to the truncated form of TrkB receptors which lack receptor tyrosine kinase activity in rodent microglial cells.

We also tested the effect of other neurotrophins, NGF and NT-3, on intracellular Ca^{2+} mobilization in rodent microglial cells. NGF and NT-3 preferentially bind to TrkA and TrkC receptors, respectively (33, 37). A brief (3 min) application of NGF (20 ng/ml) induced a transient elevation of intracellular Ca^{2+} in both 6–3 (n = 52; data not shown) and primary microglial cells (n = 68; Fig. 1*F*). In contrast, NT-3 (20 ng/ml) slightly elevated $[Ca^{2+}]i$ in both 6–3 (n = 55; data not shown) and primary microglial cells tested (n = 52; Fig. 1*F*).

Truncated TrkB-T1 receptors are expressed in rodent microglial cells

In cultured rat astrocytes, the expression of truncated TrkB-T1 receptors is >100-fold higher than that of TrkB-FL or TrkB-T2 receptors (33, 45). However, it remains unclear whether rodent microglial cells also express TrkB-T1 receptors. We used immunocytochemistry to examine the expression of TrkB-T1 and TrkB-FL receptors in rodent microglial cells. In both rat primary (Fig. 2*A*) and murine 6-3 (Fig. 2*B*) microglial cells, an Ab specific for TrkB-T1 receptor demonstrated substantial staining. In addition, an Ab to TrkB-FL receptor also stained both primary rat and murine 6-3 microglial cells (data not shown).

Next, we used RT-PCR to examine the expression of TrkB-T1 and TrkB-FL receptors in rodent microglial cells. We amplified PCR products for TrkB-T1 (Fig. 2*C*) and TrkB-FL (Fig. 2*D*) receptors in both rat primary and murine 6-3 microglial cells. Additionally, PCR products for both TrkB-T1 and TrkB-FL receptor mRNA were found in astrocytes and neurons cultured from rats (Fig. 2*E*). Thus, immunocytochemical techniques and RT-PCR revealed that both TrkB-T1 and TrkB-FL receptors were expressed in the rodent microglial cells we examined.

BDNF elevates intracellular Ca^{2+} via the activation of the phospholipase C (PLC) pathway and store-operated calcium entry in rodent microglial cells

BDNF binds to the TrkB receptor and rapidly induces the activation of intracellular signaling pathways, including PLC-γ and PI3K (38, 41). In the presence of U73122 (5 μM), a membrane-permeable specific PLC inhibitor (46), BDNF (20 ng/ml) failed to elevate $[Ca^{2+}]i$ in both 6-3 (n = 92; Fig. 3, *A* and *C*) and primary (n = 55) microglial cells. Contrastingly, in the presence of U73343 (10 μM), an inactive analog of U73122, BDNF induced a sustained increase in $[Ca^{2+}]i$ in both 6–3 (n = 30; Fig. 3*C*) and primary (n = 21) microglial cells. In the presence of LY-294002 (10 μM), a PI3K inhibitor (47), BDNF again induced a sustained increase in $[Ca^{2+}]i$ in both 6-3 (n = 45; Fig. 3*C*) and primary (n = 22) microglial cells. These results suggest that the activation of PLC but not PI3K is involved in the induction of BDNF-induced intracellular Ca^{2+} elevation in rodent microglial cells.

BDNF rapidly activates the PLC pathway, leading to the generation of inositol trisphosphate (IP_3) and the mobilization of intracellular Ca^{2+} from the endoplasmic reticulum (33, 37, 38). In the presence of thapsigargin (200 nM), which depletes intracellular Ca^{2+} stores by inhibiting endoplasmic reticulum Ca^{2+}-ATPase (48), BDNF did not elevate $[Ca^{2+}]i$ in 6-3 (n = 51; Fig. 3*C*) and primary (n = 22) microglial cells. In cells which are not excitable, including microglia, the influx of Ca^{2+} through the store-operated calcium entry (SOCE) plays a major role in intracellular Ca^{2+} signaling (26, 49). In the Ca^{2+}-free external solution, BDNF failed to elevate $[Ca^{2+}]i$ in 6-3 (n = 110; Fig. 3, *B* and *C*) and primary (n = 23) microglial cells, whereas 100 μM ATP elicited a transient increase in $[Ca^{2+}]i$ as described previously (Fig. 3*B*) (36). These results suggest that BDNF induced sustained increase in $[Ca^{2+}]i$ through the activation of PLC/IP_3/SOCE pathway in the rodent microglial cells.

We next tested the effect of 2-APB or SKF-96365, both of which are membrane-permeable inhibitors of IP_3 receptor-induced Ca^{2+} release (50), on the BDNF-induced elevation of $[Ca^{2+}]i$ in rodent microglial cells. We used these drugs because recent reports have shown that 2-APB can block the store-operated Ca^{2+} channels including transient receptor potential (TRP) channels by interacting at the outside of cell (51, 52). SKF-96365 has also been shown to be an inhibiter of TRP channels rather than that of SOCE (40, 41). In the presence of 2-APB (50 μM) or SKF-96365 (30 μM), BDNF did not induce the elevation of intracellular Ca^{2+} in 6-3 (n = 44 for 2-APB; n = 62 for SKF; Fig. 3*C*) and primary (n = 21 for 2-APB; n = 22 for SKF) rodent microglial cells. These data suggest that BDNF induced sustained increase in $[Ca^{2+}]i$ through the SOCE, possibly mediated by TRP channels, in rodent microglial cells.

BDNF activates PLC-γ via the activation of G proteins in cultured rat astrocytes (33). In the present study, application of AlF_4^- (30 μM), a general activator of heterotrimeric G proteins (53), induced an increase in basal levels of $[Ca^{2+}]i$ in the 6-3 and primary microglial cells (data not shown). BDNF (20 ng/ml) did not elevate $[Ca^{2+}]i$ in 6-3 (n = 57; Fig. 3*C*) and primary (n = 23)

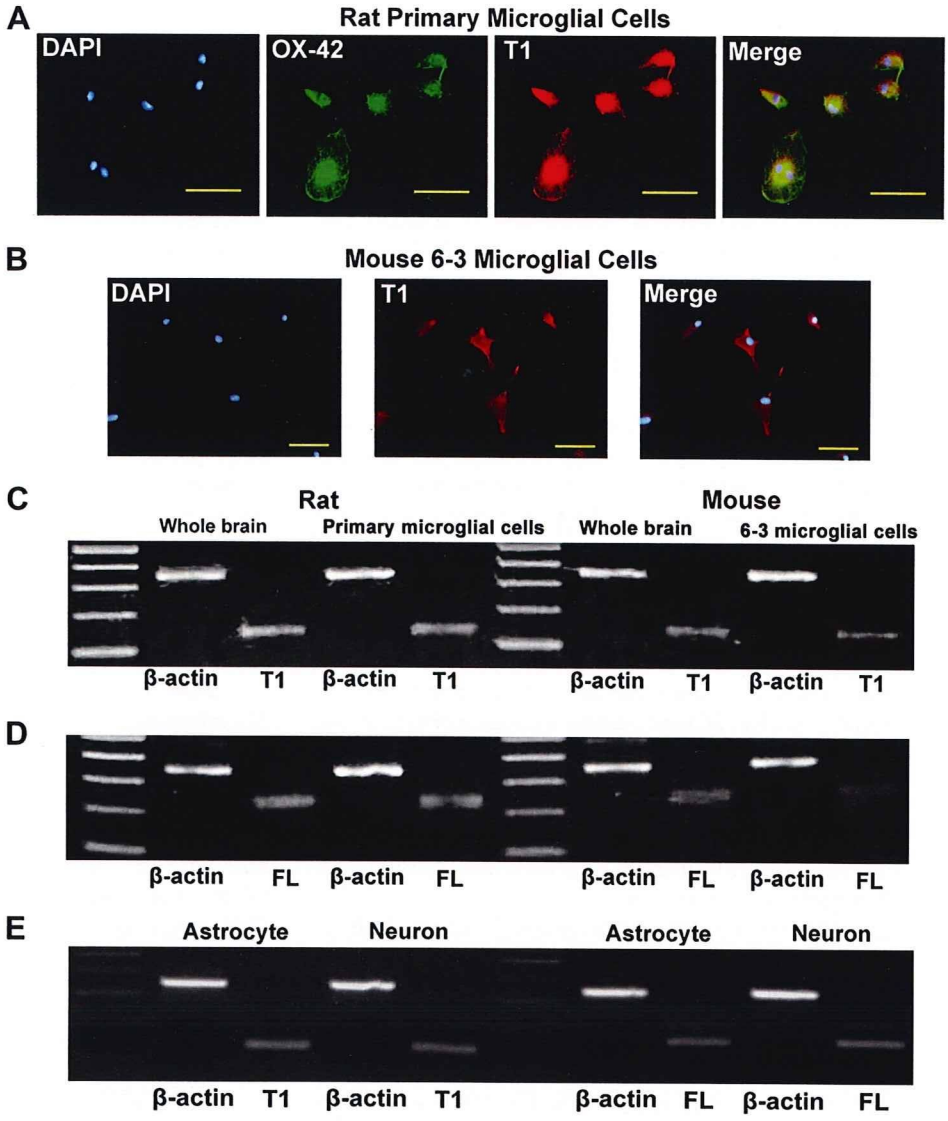

FIGURE 2. Truncated TrkB-T1 receptors are expressed in rodent microglial cells. *A*, TrkB-T1 receptors were expressed in primary rat microglial cells. In each panel, microglial cells show substantial staining of DAPI (blue), OX-42 (green), and TrkB-T1 receptors (red). *B*, TrkB-T1 receptors were expressed in murine 6-3 microglial cells. In each panel, microglial cells exhibited substantial staining of DAPI (blue) and TrkB-T1 receptors (red). Scale bar = 50 μm in *A* and *B*. *C* and *D*, The expression of TrkB-T1 (*C*) and TrkB-FL (*D*) receptor mRNA in rodent microglial cells. PCR using cDNA made from RNA isolated from the whole rat brain, primary rat microglial cells, the whole murine brain and murine 6-3 microglial cells was performed. Agarose gel electrophoresis of PCR products demonstrates a 128 bp product for the TrkB-T1 receptor (*C*) and a 195 bp product for the TrkB-FL (*D*) receptor. *E*, Expression of TrkB-T1 and TrkB-FL receptor mRNA in cultured astrocytes and neurons prepared from rats.

microglial cells in the presence of AlF_4^-. This would suggest that sustained activation of G proteins by AlF_4^- occluded BDNF-induced activation of G proteins and their downstream signaling pathways. Taken altogether, these results suggest that BDNF induced a sustained increase in $[Ca^{2+}]i$ through binding to the truncated TrkB receptors, resulting in the activation of G proteins, PLC, and SOCE in rodent microglial cells (Fig. 3*C*).

Sustained activation of SOCE contributes to the maintenance of BDNF-induced sustained intracellular Ca^{2+} elevation in rodent microglial cells

We applied the Ca^{2+}-free external solution after the onset of BDNF-induced sustained intracellular Ca^{2+} elevation to investigate the involvement of extracellular Ca^{2+} in the maintenance of long lasting $[Ca^{2+}]_i$ elevation. Removal of extracellular Ca^{2+} suppressed the $[Ca^{2+}]i$ to near basal levels in both 6-3 (n = 66; Fig. 4*A*) and primary (n = 21) microglial cells. After washing out the Ca^{2+}-free external solution, intracellular Ca^{2+} again gradually increased and persisted elevating (Fig. 4*A*).

After the onset of BDNF-induced intracellular Ca^{2+} elevation, 2-APB (50 μM) was applied and found to suppress the $[Ca^{2+}]i$ to near basal levels in the 6–3 (n = 56; Fig. 4*B*) and primary (n = 24) microglial cells. Once the 2-APB was washed out, intracellular Ca^{2+} again gradually increased and persisted elevating (Fig. 4*B*).

Moreover, SKF-96365 (30 μM) applied after the onset of BDNF-induced intracellular Ca^{2+} elevation also suppressed $[Ca^{2+}]i$ to almost basal levels in 6-3 (n = 103) and primary (n = 27; Fig. 4*C*) microglial cells. Interestingly, U73122 (10 μM) applied after the onset of BDNF-induced intracellular Ca^{2+} elevation did not affect $[Ca^{2+}]i$ in 6–3 (n = 32) and primary (n = 34; Fig. 4*D*) microglial cells.

These results indicate that sustained activation of SOCE, possibly mediated by TRP channels, occurred after a brief application of BDNF and contributed to the maintenance of BDNF-induced sustained intracellular Ca^{2+} elevation. The activation of PLC was not important for the maintenance of BDNF-induced sustained intracellular Ca^{2+} elevation in rodent microglial cells. A putative mechanism underlying the BDNF-induced sustained intracellular Ca^{2+} elevation is shown in Fig. 6 and discussed later.

Pretreatment of BDNF suppressed both the generation of NO and the IFN-γ-induced elevation of $[Ca^{2+}]i$, along with a rise in basal $[Ca^{2+}]i$ in rodent microglial cells

We observed that application of IFN-γ significantly induced NO release from 6 to 3 microglial cells as previously reported (8, 9). The 6-3 cells were pretreated with BDNF for 12 h, then treated with BDNF and IFN-γ (50 U/ml) for 48 h. Pretreatment of BDNF

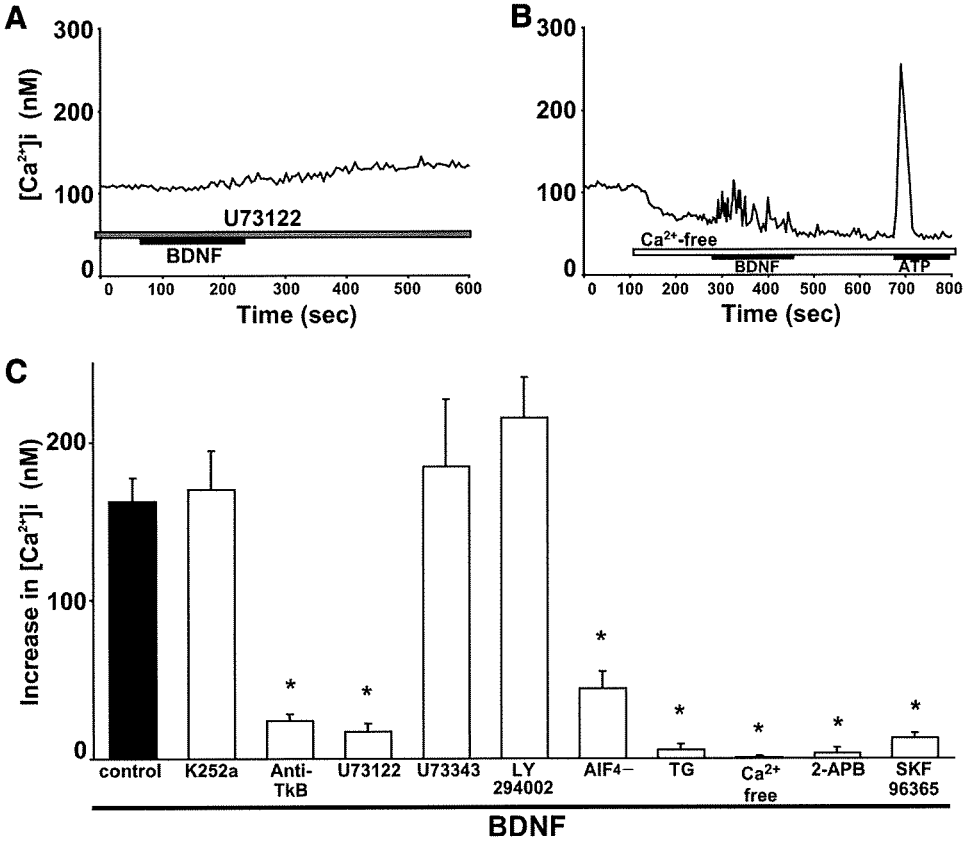

FIGURE 3. BDNF elevates intracellular Ca^{2+} through the activation of PLC and SOCE in rodent microglial cells. *A*, In the presence of 5 μM U73122, a membrane-permeable inhibitor of PLC, BDNF did not elevate $[Ca^{2+}]i$ in murine 6-3 microglial cells. *B*, In the Ca^{2+}-free external solution, BDNF did not elevate $[Ca^{2+}]i$ in murine 6-3 microglial cells. In *A* and *B*, each panel shows the average trace determined from five representative traces of $[Ca^{2+}]i$ in each condition. *C*, Histogram summarizing the effect of different manipulations on the amplitude of BDNF-induced increases in $[Ca^{2+}]i$ obtained 15 min after BDNF treatment in murine 6-3 microglial cells (values are the mean + SE).

significantly inhibited NO release in comparison to the positive control (+IFN-γ group; Fig. 5*A*), although the effect of BDNF was small. The pretreatment of BDNF with or without IFN-γ did not have any effect on cell viability in these experiments (data not shown). Additionally, BDNF itself had no effect on the release of NO without the treatment of IFN-γ (data not shown).

In microglial cells from both humans (54) and rats (9), IFN-γ rapidly induces a progressive increase in $[Ca^{2+}]i$. We measured the effect of 24-h pretreatment with BDNF (20 ng/ml) on the mobilization of intracellular Ca^{2+} induced by IFN-γ in rodent microglial cells. As shown in Fig. 5, *B* and *C*, IFN-γ (50 U/ml) rapidly increased $[Ca^{2+}]i$ in both 6-3 and primary microglial cells. Once the intracellular Ca^{2+} rose, it gradually increased without attenuation as previously shown (9, 54).

In both 6-3 and primary microglial cells which were pretreated with BDNF, IFN-γ (50 U/ml) also induced a sustained intracellular

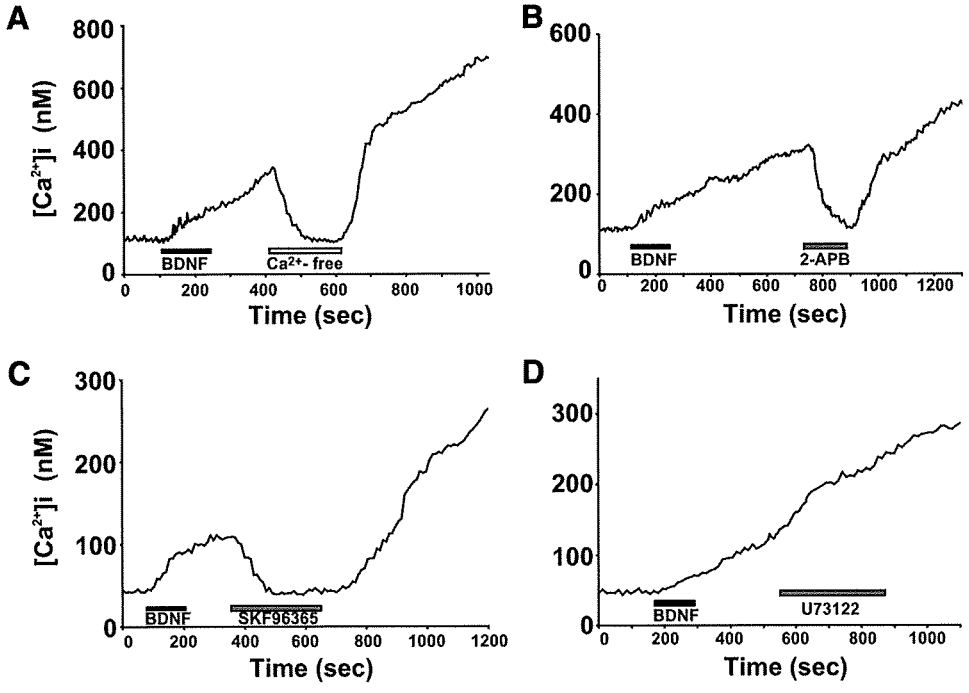

FIGURE 4. Sustained activation of SOCE contributes to the maintenance of BDNF-induced sustained intracellular Ca^{2+} elevation in rodent microglial cells. *A* and *B*, An average trace showing the effect of the Ca^{2+}-free external solution (*A*) or 50 μM 2-APB (*B*) after the onset of BDNF-induced sustained elevation of $[Ca^{2+}]i$ in murine 6-3 microglial cells. *C* and *D*, An average trace showing the effect of 30 μM SKF-96365 (*C*) or 10 μM U73122 (*D*) following the onset of BDNF-induced sustained elevation of $[Ca^{2+}]i$ in primary rat microglial cells. Each panel demonstrates the average trace determined from five representative traces of $[Ca^{2+}]i$ in each condition.

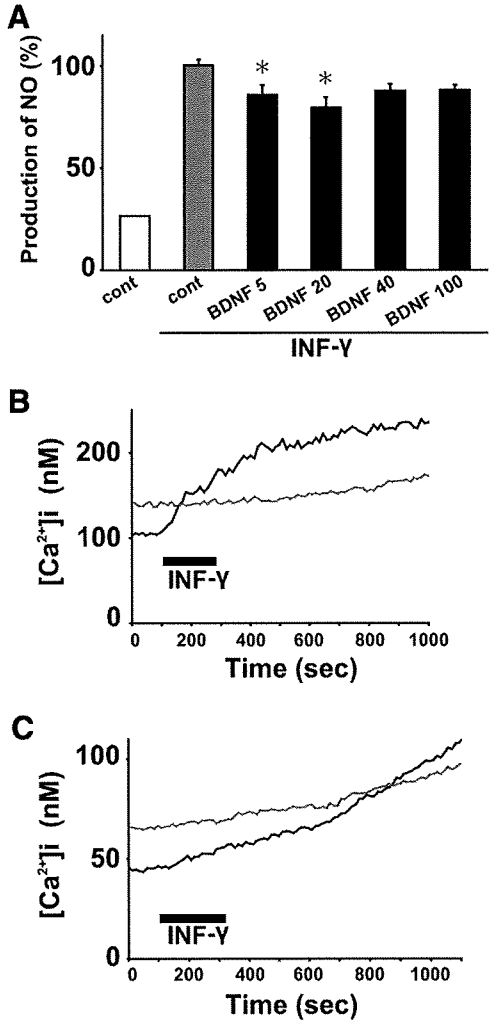

FIGURE 5. Pretreatment of BDNF suppressed both the generation of NO and the IFN-γ-induced elevation of $[Ca^{2+}]i$, along with a rise in basal $[Ca^{2+}]i$ in rodent microglial cells. *A*, Bar graphs demonstrating pretreatment with BDNF inhibited the release of NO from murine microglial cells activated by IFN-γ. *, $p < 0.05$ (Turkey). *B* and *C*, Average traces showing 24 h pretreatment with BDNF suppressed the 50 U/ml IFN-γ-induced increase in $[Ca^{2+}]i$, along with an elevation of basal levels of $[Ca^{2+}]i$ in murine 6-3 (*B*) and primary rat (*C*) microglial cells (black line, control; gray line, + BDNF). Each panel shows the average trace determined from five representative traces of $[Ca^{2+}]i$ in each condition.

Ca^{2+} elevation (Fig. 5, *B* and *C*). However, pretreatment of BDNF significantly reduced the amplitude of IFN-γ-induced increase in $[Ca^{2+}]i$ at 12 min after a 3 min treatment of IFN-γ in both 6–3 (102.4 ± 6.9 nM, $n = 140$ in control; 32.5 ± 3.0 nM, $n = 33$ in BDNF; $p < 0.001$) and primary (70.8 ± 4.8 nM, $n = 33$ in control; 29.9 ± 3.3 nM, $n = 46$ in BDNF; $p < 0.001$) microglial cells. The basal level of $[Ca^{2+}]i$ was elevated in microglial cells pretreated with BDNF in 6-3 (115.1 ± 1.0 nM in control; 144.3 ± 8.1 nM in BDNF; $p < 0.001$) and primary (45.0 ± 0.5 nM in control; 65.5 ± 1.0 nM in BDNF; $p < 0.001$; Fig. 5, *B* and *C*) microglial cells.

Discussion

In this study, we sought direct evidence that microglia are able to respond to BDNF by examining whether BDNF affects intracellular Ca^{2+} mobilization in rodent microglial cells. We found that BDNF induced a sustained increase in $[Ca^{2+}]i$ through the binding to the truncated TrkB receptors, resulting in the activation of the PLC pathway and SOCE in rodent microglial cells. RT-PCR and

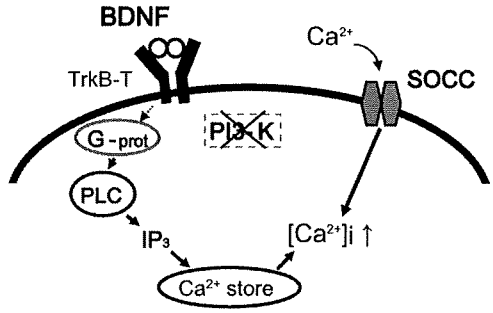

FIGURE 6. Schematic illustration demonstrating the underlying mechanism of BDNF-induced sustained increase of $[Ca^{2+}]i$ in rodent microglial cells. BDNF induces a sustained increase in $[Ca^{2+}]i$ through binding of the truncated TrkB receptors (TrkB-T), resulting in activation of the PLC pathway and SOCE. Sustained activation of SOCC, such as TRP channels, occurs after a brief treatment with BDNF and contributes to the maintenance of BDNF-induced sustained intracellular Ca^{2+} elevation. PLC, phospholipase C; G-prot, G protein; SOCC, store-operated calcium channel; PI3K, phosphatidylinositol 3 kinase.

immunocytochemical techniques revealed that truncated TrkB-T1 receptors were highly expressed in rodent microglial cells. Sustained activation of SOCE occurred after a brief treatment with BDNF and contributed to the maintenance of BDNF-induced sustained intracellular Ca^{2+} elevation. Pretreatment of BDNF significantly suppressed the release of NO from activated microglia. Pretreatment of BDNF also suppressed the IFN-γ-induced increase in $[Ca^{2+}]i$, along with a rise in basal levels of $[Ca^{2+}]i$ in rodent microglial cells. To the best of our knowledge, this is the first report showing that BDNF rapidly elevates $[Ca^{2+}]_i$ in rodent microglial cells.

TrkB-T1 receptors are predominantly expressed in rat astrocytes (33), while the expression of TrkB-FL receptors is up-regulated after brain injury (55). Although the physiological significance of truncated TrkB receptors is still unknown (38, 56), several studies support the importance of TrkB-T1 receptors in the CNS. In cultured rat astrocytes, TrkB-T1 receptors mediate the BDNF-induced elevation of $[Ca^{2+}]i$ (33) and are involved in their morphological changes (45). Carim-Todd et al. (56) have recently reported that TrkB-T1-deficient mice develop normally but have increased anxiety-like behavior, accompanied by morphological abnormalities in the dendrites of neurons in the basolateral amygdala. In the present study, we demonstrated that TrkB-T1 receptors were highly expressed in rodent microglial cells (Fig. 2). We also observed that BDNF induced a sustained elevation of intracellular Ca^{2+} through the binding to the truncated TrkB receptors in rodent microglial cells. We need further studies to elucidate the physiological significance of truncated TrkB receptors in rodent microglial cells.

A brief application of 100 μM ATP in rodent microglial cells induced only a transient intracellular Ca^{2+} elevation (Fig. 1*B*, *inset*). A low concentration of ATP mainly activates purinergic (P2Y) receptors that lead to the activation of PLC and SOCE, resulting in a transient elevation of $[Ca^{2+}]i$ (57). BDNF induces a transient intracellular Ca^{2+} elevation in cultured rat astrocytes, through the binding to the truncated TrkB receptors, leading to the activation of PLC and SOCE (33). We also observed that BDNF-activated PLC and SOCE through the binding to truncated TrkB receptors in rodent microglial cells, whereas BDNF induced a sustained elevation of $[Ca^{2+}]i$. Activation of microglia, including proliferation, release of cytokines and reactive oxygen species, migration, ramification, and de-ramification, are frequently accompanied by a sustained increase in $[Ca^{2+}]i$ (26, 27). These results

suggest that microglia may have their own activation mechanism underlying the BDNF-induced sustained increase in $[Ca^{2+}]i$. Additionally, BDNF-induced sustained increases in $[Ca^{2+}]i$ may play an important role in the activation of microglia.

In PC12 cells, a 1–2 min treatment of NGF rapidly phosphorylates PLC-γ through the activation of the TrkA receptor tyrosine kinase, in which the autophosphorylation of the TrkA receptor and the phosphorylation of PLC-γ are sustained for up to 30 min and 2 h, respectively (58). We observed that the activation of PLC was not important for the maintenance of BDNF-induced sustained intracellular Ca^{2+} elevation (Fig. 4*D*). A sustained activation of SOCE, possibly mediated by TRP channels, could occur after a brief treatment with BDNF and then contribute to the maintenance of BDNF-induced sustained intracellular Ca^{2+} elevation in rodent microglial cells.

Using rat hippocampal slice cultures, BDNF application to the apical dendrites of CA1 pyramidal neurons induces a slow and sustained nonselective cationic current mediated by SKF96365-sensitive TRPC3 channels (41). TRPC channels are necessary for BDNF to induce chemoattractive turning of the growth cone (40) or to increase dendritic spine density (41) in neurons. In nonexcitable cells, such as microglia, influx of Ca^{2+} through the TRP channels plays an important role in intracellular calcium signaling (26, 49) and in many inflammatory processes, including the activation of microglia (59). TRP channels also contribute to the alteration of intracellular Ca^{2+} signaling in patients suffering from bipolar disorder (30, 59). We need to further examine the mechanism underlying the maintenance of BDNF-induced sustained increase in $[Ca^{2+}]i$ in rodent microglial cells.

Pretreatment with BDNF suppresses the release of NO from cultured rat microglia stimulated by LPS (60). In the present study, we observed that pretreatment with BDNF significantly suppressed the release of NO from murine microglial cells activated by IFN-γ, although the effect of BDNF was small. In murine microglial cells, risperidone significantly inhibits the expression of inducible NO synthase (Ref. 8), thus BDNF might also suppress the expression of inducible NO synthase in IFN-γ-stimulated murine microglial cells.

The biological effects of IFN-γ are elicited through the activation of intracellular signaling pathways, including the JAK-STAT pathway. The phosphorylated STAT1 homodimer translocates to the nucleus and initiates gene transcription (61). In NIH 3T3 cells, influx of Ca^{2+} induced by IFN-γ is required for the ser-727 phosphorylation of STAT1 (62). In this study, we observed that pretreatment with BDNF significantly suppressed the IFN-γ-induced elevation of $[Ca^{2+}]i$, along with a rise in basal levels of $[Ca^{2+}]i$ in rodent microglial cells (Fig. 5, *B* and *C*). A 24 h pretreatment with LPS on cultured murine microglial cells suppressed UTP- or complement factor 5a-induced elevation of $[Ca^{2+}]i$, but increased basal levels of $[Ca^{2+}]i$ (63). It was also demonstrated that cotreatment with LPS and BAPTA-AM, a membrane-permeable chelator of intracellular Ca^{2+}, restored the baseline $[Ca^{2+}]i$ to normal levels and re-established the UTP-induced elevation of $[Ca^{2+}]i$. Although BAPTA-AM inhibited the release of NO and cytokines from LPS-activated microglia, ionomycin, a calcium ionophore that elevates $[Ca^{2+}]i$, had no effect on the release of NO and cytokines from activated microglia. This is indicative that an increase in basal $[Ca^{2+}]i$ is required, but by itself is not sufficient, for the release of NO and cytokines from activated microglia (63). We have also shown that BAPTA-AM significantly inhibits the release of NO from IFN-γ-activated murine microglial cells (9).

BDNF might inhibit IFN-γ-induced microglial activation through the suppression of IFN-γ-induced elevation of $[Ca^{2+}]i$ in rodent microglial cells. BDNF-induced elevation of basal levels of $[Ca^{2+}]i$ could regulate the microglial intracellular signal transduction. A recent report by Hall et al. (64) demonstrated the implication of the basal level of $[Ca^{2+}]i$ in the activation of rodent microglia, including NO production.

Microglia are predominantly found in the gray matter, with the highest concentration in the hippocampus, olfactory telencephalon, basal ganglia, and substantia nigra of the adult mammalian brain (1). There is increasing evidence that suggests that pathophysiology of neuropsychiatric disorders, including schizophrenia (4) and depression (5, 6), are related to the inflammatory responses mediated by microglia. BDNF is most abundantly expressed in the hippocampus and cerebral cortex (24) and is also involved in the pathophysiology of neuropsychiatric disorders (20–24). We have recently reported that pretreatment with antidepressants (7) or antipsychotics (8, 9) significantly inhibits the release of NO and cytokines from activated microglia, respectively. In this study, we observed that pretreatment with BDNF significantly inhibited the release of NO from activated microglia (Fig. 5*A*). This would suggest that BDNF might have an anti-inflammatory effect through the inhibition of microglial activation and could be useful for the treatment of neuropsychiatric disorders.

We have shown direct evidence that rodent microglial cells are able to respond to BDNF, which may be important for the regulation of inflammatory responses and may also be involved in the pathophysiology or treatment of neuropsychiatric disorders.

Acknowledgments

We thank Prof. Makoto Sawada of Nagoya University for providing us with the microglial cell line, 6-3.

Disclosures

The authors have no financial conflict of interest.

References

1. Block, M. L., L. Zecca, and J. S. Hong. 2007. Microglia-mediated neurotoxicity: uncovering the molecular mechanisms. *Nat. Rev. Neurosci.* 8: 57–69.
2. Hanisch, U. K., and H. Kettenmann. 2007. Microglia: active sensor and versatile effector cells in the normal and pathologic brain. *Nat. Neurosci.* 10: 1387–1394.
3. Nimmerjahn, A., F. Kirchhoff, and F. Helmchen. 2005. Resting microglial cells are highly dynamic surveillants of brain parenchyma in vivo. *Science* 308: 1314–1318.
4. van Berckel, B. N., M. G. Bossong, R. Boellaard, R. Kloet, A. Schuitemaker, E. Caspers, G. Luurtsema, A. D. Windhorst, W. Cahn, A. A. Lammertsma, and R. S. Kahn. 2008. Microglia activation in recent-onset schizophrenia: a quantitative (R)-[11C]PK11195 positron emission tomography study. *Biol. Psychiatry* 64: 820–882.
5. Dantzer, R., J. C. O'Connor, G. G. Freund, R. W. Johnson, and K. W. Kelley. 2008. From inflammation to sickness and depression: when the immune system subjugates the brain. *Nat. Rev. Neurosci.* 9: 46–56.
6. Müller, N., and M. J. Schwarz. 2008. A psychoneuroimmunological perspective to Emil Kraepelins dichotomy: schizophrenia and major depression as inflammatory CNS disorders. *Eur. Arch. Psychiatry Clin. Neurosci.* 258 (Suppl. 2): 97–106.
7. Hashioka, S., A. Klegeris, A. Monji, T. Kato, M. Sawada, P. L. McGeer, and S. Kanba. 2007. Antidepressants inhibit interferon-γ-induced microglial production of IL-6 and nitric oxide. *Exp. Neurol.* 206: 33–42.
8. Kato, T., A. Monji, S. Hashioka, and S. Kanba. 2007. Risperidone significantly inhibits interferon-γ-induced microglial activation in vitro. *Schizophr. Res.* 92: 108–115.
9. Kato, T., Y. Mizoguchi, A. Monji, H. Horikawa, S. O. Suzuki, Y. Seki, T. Iwaki, S. Hashioka, and S. Kanba. 2008. Inhibitory effects of aripiprazole on interferon-γ-induced microglial activation via intracellular Ca^{2+} regulation in vitro. *J. Neurochem.* 106: 815–825.
10. Poo, M. M. 2001. Neurotrophins as synaptic modulators. *Nat. Rev. Neurosci.* 2: 24–32.
11. Lu, B., P. T. Pang, and N. H. Woo. 2005. The yin and yang of neurotrophin action. *Nat. Rev. Neurosci.* 6: 603–614.
12. Mizoguchi, Y., T. Kanematsu, M. Hirata, and J. Nabekura. 2003. A rapid increase in the total number of cell surface functional $GABA_A$ receptors induced by brain-derived neurotrophic factor in rat visual cortex. *J. Biol. Chem.* 278: 44097–44102.
13. Mizoguchi, Y., H. Ishibashi, and J. Nabekura. 2003. The action of BDNF on GABA(A) currents changes from potentiating to suppressing during maturation of rat hippocampal CA1 pyramidal neurons. *J. Physiol.* 548: 703–709.
14. Mizoguchi, Y., A. Kitamura, H. Wake, H. Ishibashi, M. Watanabe, T. Nishimaki, and J. Nabekura. 2006. BDNF occludes GABA receptor-mediated inhibition of

GABA release in rat hippocampal CA1 pyramidal neurons. *Eur. J. Neurosci.* 24: 2135–2144.
15. Elkabes, S., E. M. DiCicco-Bloom, and I. B. Black. 1996. Brain microglia/macrophages express neurotrophins that selectively regulate microglial proliferation and function. *J. Neurosci.* 16: 2508–2521.
16. Nakajima, K., S. Honda, Y. Tohyama, Y. Imai, S. Kohsaka, and T. Kurihara. 2001. Neurotrophin secretion from cultured microglia. *J. Neurosci. Res.* 65: 322–331.
17. Batchelor, P. E., G. T. Liberatore, J. Y. Wong, M. J. Porritt, F. Frerichs, G. A. Donnan, and D. W. Howells. 1999. Activated macrophages and microglia induce dopaminergic sprouting in the injured striatum and express brain-derived neurotrophic factor and glial cell line-derived neurotrophic factor. *J. Neurosci.* 19: 1708–1716.
18. Coull, J. A., S. Beggs, D. Boudreau, D. Boivin, M. Tsuda, K. Inoue, C. Gravel, M. W. Salter, and Y. De Koninck. 2005. BDNF from microglia causes the shift in neuronal anion gradient underlying neuropathic pain. *Nature* 438: 1017–1021.
19. Zhang, J., C. Geula, C. Lu, H. Koziel, L. M. Hatcher, and F. J. Roisen. 2003. Neurotrophins regulate proliferation and survival of two microglial cell lines in vitro. *Exp. Neurol.* 183: 469–481.
20. Angelucci, F., S. Brenè, and A. A. Mathé. 2005. BDNF in schizophrenia, depression and corresponding animal models. *Mol. Psychiatry* 10: 345–352.
21. Berton, O., and E. J. Nestler. 2006. New approaches to antidepressant drug discovery: beyond monoamines. *Nat. Rev. Neurosci.* 7: 137–151.
22. Duman, R. S., and L. M. Monteggia. 2006. A neurotrophic model for stress-related mood disorders. *Biol. Psychiatry* 59: 1116–1127.
23. Li, Y., B. W. Luikart, S. Birnbaum, J. Chen, C. H. Kwon, S. G. Kernie, R. Bassel-Duby, and L. F. Parada. 2008. TrkB regulates hippocampal neurogenesis and governs sensitivity to antidepressive treatment. *Neuron* 59: 399–412.
24. Sen, S., R. Duman, and G. Sanacora. 2008. Serum brain-derived neurotrophic factor, depression, and antidepressant medications: meta-analyses and implications. *Biol. Psychiatry* 64: 527–532.
25. Berridge, M. J., M. D. Bootman, and H. L. Roderick. 2003. Calcium signalling: dynamics, homeostasis and remodelling. *Nat. Rev. Mol. Cell Biol.* 4: 517–529.
26. Eder, C. 2005. Regulation of microglial behavior by ion channel activity. *J. Neurosci. Res.* 81: 314–321.
27. Färber, K., and H. Kettenmann. 2006. Functional role of calcium signals for microglial function. *Glia* 54: 656–665.
28. Trang, T., S. Beggs, X. Wan, and M. W. Salter. 2009. P2X4-receptor-mediated synthesis and release of brain-derived neurotrophic factor in microglia is dependent on calcium and p38-mitogen-activated protein kinase activation. *J. Neurosci.* 29: 3518–3528.
29. Lidow, M. S. 2002. Calcium signaling dysfunction in schizophrenia: a unifying approach. *Brain Res. Brain Res. Rev.* 43: 70–84.
30. Kato, T. 2008. Role of mitochondrial DNA in calcium signaling abnormality in bipolar disorder. *Cell Calcium* 44: 92–102.
31. Mizoguchi, Y., A. Monji, and J. Nabekura. 2002. Brain-derived neurotrophic factor induces long-lasting Ca^{2+}-activated K^+ currents in rat visual cortex neurons. *Eur. J. Neurosci.* 16: 1417–1424.
32. Lang, S. B., V. Stein, T. Bonhoeffer, and C. Lohmann. 2007. Endogenous brain-derived neurotrophic factor triggers fast calcium transients at synapses in developing dendrites. *J. Neurosci.* 27: 1097–1105.
33. Rose, C. R., R. Blum, B. Pichler, A. Lepier, K. W. Kafitz, and A. Konnerth. 2003. Truncated TrkB-T1 mediates neurotrophin-evoked calcium signalling in glia cells. *Nature* 426: 74–78.
34. Kanzawa, T., M. Sawada, K. Kato, K. Yamamoto, H. Mori, and R. Tanaka. 2000. Differentiated regulation of allo-antigen presentation by different types of murine microglial cell lines. *J. Neurosci. Res.* 62: 383–388.
35. Grynkiewicz, G., M. Poenie, and R. Y. Tsien. 1985. A new generation of Ca^{2+} indicators with greatly improved fluorescence properties. *J. Biol. Chem.* 60: 3440–3450.
36. McLarnon, J. G., L. Zhang, V. Goghari, Y. B. Lee, W. Walz, C. Krieger, and S. U. Kim. 1999. Effects of ATP and elevated K^+ on K^+ currents and intracellular Ca^{2+} in human microglia. *Neuroscience* 91: 343–352.
37. Patapoutian, A., and L. F. Reichardt. 2001. Trk receptors: mediators of neurotrophin action. *Curr. Opin. Neurobiol.* 11: 272–280.
38. Rose, C. R., R. Blum, K. W. Kafitz, Y. Kovalchuk, and A. Konnerth. 2004. From modulator to mediator: rapid effects of BDNF on ion channels. *Bioessays* 26: 1185–1194.
39. Tapley, P., F. Lamballe, and M. Barbacid. 1992. K252a is a selective inhibitor of the tyrosine protein kinase activity of the trk family of oncogenes and neurotrophin receptors. *Oncogene* 7: 371–381.
40. Li, Y., Y. C. Jia, K. Cui, N. Li, Z. Y. Zheng, Y. Z. Wang, and X. B. Yuan. 2005. Essential role of TRPC channels in the guidance of nerve growth cones by brain-derived neurotrophic factor. *Nature* 434: 894–898.
41. Amaral, M. D., and L. Pozzo-Miller. 2007. TRPC3 channels are necessary for brain-derived neurotrophic factor to activate a nonselective cationic current and to induce dendritic spine formation. *J. Neurosci.* 27: 5179–5189.
42. Kang, H., A. A. Welcher, D. Shelton, and E. M. Schuman. 1997. Neurotrophins and time: different roles for TrkB signaling in hippocampal long-term potentiation. *Neuron* 19: 653–664.
43. Baldelli, P., J. M. Hernandez-Guijo, V. Carabelli, and E. Carbone. 2005. Brain-derived neurotrophic factor enhances GABA release probability and nonuniform distribution of N- and P/Q-type channels on release sites of hippocampal inhibitory synapses. *J. Neurosci.* 25: 3358–3368.
44. Klein, R., D. Conway, L. F. Parada, and M. Barbacid. 1990. The trkB tyrosine protein kinase gene codes for a second neurogenic receptor that lacks the catalytic kinase domain. *Cell* 61: 647–656.
45. Ohira, K., H. Kumanogoh, Y. Sahara, K. J. Homma, H. Hirai, S. Nakamura, and M. Hayashi. 2005. A truncated tropomyosin-related kinase B receptor, T1, regulates glial cell morphology via Rho GDP dissociation inhibitor 1. *J. Neurosci.* 25: 1343–1353.
46. Yule, D. I., and J. A. Williams. 1992. U73122 inhibits Ca^{2+} oscillations in response to cholecystokinin and carbachol but not to JMV-180 in rat pancreatic acinar cells. *J. Biol. Chem.* 267: 13830–13835.
47. Vlahos, C. J., W. F. Matter, K. Y. Hui, and R. F. Brown. 1994. A specific inhibitor of phosphatidylinositol 3-kinase, 2-(4-morpholinyl)-8-phenyl-4H-1-benzopyran-4-one (LY294002). *J. Biol. Chem.* 269: 5241–5248.
48. Thastrup, O., P. J. Cullen, B. K. Drøbak, M. R. Hanley, and A. P. Dawson. 1990. Thapsigargin, a tumor promoter, discharges intracellular Ca^{2+} stores by specific inhibition of the endoplasmic reticulum Ca^{2+}-ATPase. *Proc. Natl. Acad. Sci. USA* 87: 2466–2470.
49. Möller, T. 2002. Calcium signaling in microglial cells. *Glia* 40: 184–194.
50. Merritt, J. E., W. P. Armstrong, C. D. Benham, T. J. Hallam, R. Jacob, A. Jaxa-Chamiec, B. K. Leigh, S. A. McCarthy, K. E. Moores, and T. J. Rink. 1990. SKF 96365, a novel inhibitor of receptor-mediated calcium entry. *Biochem. J.* 271: 515–522.
51. Bootman, M. D., T. J. Collins, L. Mackenzie, H. L. Roderick, M. J. Berridge, and C. M. Peppiatt. 2002. 2-aminoethoxydiphenyl borate (2-APB) is a reliable blocker of store-operated Ca^{2+} entry but an inconsistent inhibitor of $InsP_3$-induced Ca^{2+} release. *FASEB J.* 16: 1145–1150.
52. Togashi, K., H. Inada, and M. Tominaga. 2008. Inhibition of the transient receptor potential cation channel TRPM2 by 2-aminoethoxydiphenyl borate (2-APB). *Br. J. Pharmacol.* 153: 1324–1330.
53. Bigay, J., P. Deterre, C. Pfister, and M. Chabre. 1987. Fluoride complexes of aluminium or beryllium act on G-proteins as reversibly bound analogues of the γ phosphate of GTP. *EMBO J.* 6: 2907–2913.
54. Franciosi, S., H. B. Choi, S. U. Kim, and J. G. McLarnon. 2002. Interferon-γ acutely induces calcium influx in human microglia. *J. Neurosci. Res.* 69: 607–613.
55. Climent, E., M. Sancho-Tello, R. Miñana, D. Barettino, and C. Guerri. 2000. Astrocytes in culture express the full-length Trk-B receptor and respond to brain derived neurotrophic factor by changing intracellular calcium levels: effect of ethanol exposure in rats. *Neurosci. Lett.* 288: 53–56.
56. Carim-Todd, L., K. G. Bath, G. Fulgenzi, S. Yanpallewar, D. Jing, C. A. Barrick, J. Becker, H. Buckley, S. G. Dorsey, F. S. Lee, and L. Tessarollo. 2009. Endogenous truncated TrkB.T1 receptor regulates neuronal complexity and TrkB kinase receptor function in vivo. *J. Neurosci.* 29: 678–685.
57. McLarnon, J. G. 2005. Purinergic mediated changes in Ca^{2+} mobilization and functional responses in microglia: effects of low levels of ATP. *J. Neurosci. Res.* 81: 349–356.
58. Choi, D. Y., J. J. Toledo-Aral, R. Segal, and S. Halegoua. 2001. Sustained signaling by phospholipase C-γ mediates nerve growth factor-triggered gene expression. *Mol. Cell Biol.* 21: 2695–2705.
59. Nilius, B., G. Owsianik, T. Voets, and J. A. Peters. 2007. Transient receptor potential cation channels in disease. *Physiol. Rev.* 87: 165–217.
60. Nakajima, K., Y. Kikuchi, E. Ikoma, S. Honda, M. Ishikawa, Y. Liu, and S. Kohsaka. 1998. Neurotrophins regulate the function of cultured microglia. *Glia* 24: 272–289.
61. Gough, D. J., D. E. Levy, R. W. Johnstone, and C. J. Clarke. 2008. IFNγ signaling-does it mean JAK-STAT? *Cytokine Growth Factor Rev.* 19: 383–394.
62. Nair, J. S., C. J. DaFonseca, A. Tjernberg, W. Sun, J. E. Darnell, Jr., B. T. Chait, and J. J. Zhang. 2002. Requirement of Ca^{2+} and CaMKII for Stat1 Ser-727 phosphorylation in response to IFN-γ. *Proc. Natl. Acad. Sci. USA* 99: 5971–5976.
63. Hoffmann, A., O. Kann, C. Ohlemeyer, U. K. Hanisch, and H. Kettenmann. 2003. Elevation of basal intracellular calcium as a central element in the activation of brain macrophages (microglia): suppression of receptor-evoked calcium signaling and control of release function. *J. Neurosci.* 23: 4410–4419.
64. Hall, A. A., Y. Herrera, C. T. Ajmo, Jr., J. Cuevas, and K. R. Pennypacker. 2009. Sigma receptors suppress multiple aspects of microglial activation. *Glia* 57: 744–754.

Progress in Neuro-Psychopharmacology & Biological Psychiatry 33 (2009) 308–311

Contents lists available at ScienceDirect

Progress in Neuro-Psychopharmacology & Biological Psychiatry

journal homepage: www.elsevier.com/locate/pnpbp

Effect of yokukansan on the behavioral and psychological symptoms of dementia in elderly patients with Alzheimer's disease

Akira Monji [a,*], Masashi Takita [b,1], Takaaki Samejima [c], Toshihiro Takaishi [c], Kazuhito Hashimoto [d], Hiroyuki Matsunaga [e], Mariko Oda [f], Yasuhisa Sumida [g], Yoshito Mizoguchi [a], Takahiro Kato [a], Hideki Horikawa [a], Shigenobu Kanba [a]

[a] Department of Neuropsychiatry, Graduate School of Medical Sciences, Kysushu University, 3-1-1 Maidashi, Higashi-ku, Fukuoka 812-8582, Japan
[b] Imazu Red Cross Hospital, 377 Imazu, Nishiku-ku, Fukuoka 819-0165, Japan
[c] Sameshima Hospital, 272 Osoekawa, Fujicho, Saga 840-0521, Japan
[d] Seiyu Hospital, 5457 Kawakubo, Kuboizumicho, Saga 849-0901, Japan
[e] Hayatsue Hospital, 827 Fukudomi, Kawasoe, Saga 840-2201, Japan
[f] Nakataku Hospital, 2512-24 Takubaru, Kitatakucho, Taku, Saga 846-0003, Japan
[g] Sumida Hospital, 1423 Amasumi, Wakamatsu-ku, Kitakyushu, Fukuoka 808-0122, Japan

ARTICLE INFO

Article history:
Received 16 October 2008
Received in revised form 15 December 2008
Accepted 15 December 2008
Available online 24 December 2008

Keywords:
Alzheimer's disease (AD)
Behavioral and psychological symptoms of dementia (BPSD)
Herbal medicine
Sulpiride
Yokukansan

ABSTRACT

Objective: The aim of this study was to investigate the effects of yokukansan (YKS) on the behavioral and psychological symptoms of dementia (BPSD) in elderly patients with Alzheimer's disease (AD).
Methods: Fifteen patients with AD (mean age: 80.2±4.0 years) participated in the study. The Mini-Mental State Examination (MMSE) was used for the assessment of cognitive function. BPSD were evaluated using the Neuropsychiatric Inventory (NPI). The Barthel Index was used for the assessment for the activities of daily living (ADL). The treatment with YKS along with sulpiride, a dopamine D_2 selective antipsychotic, was performed for 12 weeks.
Results: Fourteen patients completed the trial. After the 12 weeks of treatment with YKS, significant improvement of the mean NPI score was observed while no significant improvement was observed in the control group. The average dose of sulpiride at the end of the present study was less in the YKS group than in the control group. The MMSE results did not change either in the YKS group or in the control group. The Barthel Index did not significantly change either in the YKS group or in the control group. No serious adverse effects were noted.
Conclusions: Twelve weeks of the YKS treatment significantly improved BPSD with less antipsychotics in elderly patients with AD. The YKS treatment did not cause any cognitive decline or ADL decline and no serious adverse effects were noted. The present study suggests that YKS is beneficial for the treatment of BPSD and that it can possibly reduce the doses of antipsychotics required for the treatment of BPSD. Further studies with larger patient populations using a double-blind placebo-controlled design should be performed.

1. Introduction

Patients with dementia experience progressive cognitive impairments such as memory deficits and impaired executive functioning. The behavioral and psychological symptoms of dementia (BPSD) are also commonly seen in patients with Alzheimer's disease (AD) and other types of dementia. It is estimated that 60–80% of patients with dementia have BPSD at any one time (Lawlor, 2002). Cognitive failure is not, in itself, a sufficient explanation for functional disability or impaired quality of life for people with dementia. BPSD often causes considerable caregiver stress and hastens institutionalization of patients with dementia. Relatives and caregivers are thus likely to identify BPSD as the most important features of dementia (McKeith and Cummings, 2005; Jeste et al., 2008). While there have been several studies of pharmacological interventions for BPSD, the strategy of treatment has not been sufficiently established. Pharmacological interventions including antipsychotics and acetylcholine esterase inhibitors (AchEI) have been investigated, but elderly patients with dementia are particularly sensitive to the adverse effects such as extrapyramidal symptoms and cognitive decline. Moreover, concerns have been recently expressed regarding an increased risk of cerebrovascular adverse events (CVAEs) in elderly patients with dementia treated with antipsychotics (Schneider et al., 2006; Rainer

Abbreviations: YKS, yokukansan; BPSD, behavioral and psychological symptoms of dementia; MMSE, Mini-Mental State Examination; NPI, Neuropsychiatric Inventory; AD, Alzheimer's disease.

* Corresponding author. Fax: +81 92 642 5644.
E-mail address: amonji@hf.rim.or.jp (A. Monji).
[1] Present address: Takita Memory Mental Clinic, 5-13-8 Muromi, Sawaraku-ku, Fukuoka 814-0015, Japan.

0278-5846/$ – see front matter © 2008 Elsevier Inc. All rights reserved.
doi:10.1016/j.pnpbp.2008.12.008

Table 1
The demographic data of the patients

Subjects(n)	YKS group 10	Control 5	Total 15	*P* Value
Age(mean±SD)	80.8±4.7	79.0±2.0	80.2±4.0	Wilcoxon test $p=0.175$
Sex(male/female)	2/8	0/5	2/13	Fisher excact test $p=0.524$
Body weight(mean±SD)	44.5±8.2	46.3±3.3	45.1±6.9	Wilcoxon test $p=0.582$
Complication (presence/absence)	5/5	4/1	9/6	Fisher excact test $p=0.580$
NPI(total)	26.7±15.7	22.4±12.8	25.3±14.5	Wilcoxon test $p=0.425$
Barthel Index	77.5±16.7	63.0±34.0	72.7±23.7	Wilcoxon test $p=0.620$
MMSE	15.1±4.0	16.4±3.5	15.5±38	Wilcoxon test $p=0.423$

et al., 2007; Jeste et al., 2008; Kuehn, 2008; Sultzer et al., 2008). Clinicians and caregivers are left with unclear choices in treatment of BPSD. A systematic review indicated that some herbs and herbal formations were useful for the treatment of cognitive impairments of AD (Dos Santos-Neto et al., 2006). Yi-Gan San (yokukansan in Japanese) was developed in 1555 by Xue Kai as a remedy for restlessness and agitation in children. A recent report suggests the involvement of the 5-HT system in the psychopharmacological effects of yokukansan (YKS) (Egashira et al., 2008). The clinical efficacy and safety of YKS for improvement of cognitive function, BPSD, and activities of daily living (ADL) have been reported (Iwasaki et al., 2005a,b; Shinno et al., 2007, 2008). These studies included patients with dementia other than AD. The aim of this study was to investigate the effects of YKS on BPSD in patients with AD. We also tested for the presence of adverse effects during YKS administration.

2. Methods

2.1. Subjects

The subjects were patients admitted to Kyushu University-affiliated Hospitals. The data were collected from January 2006 to March 2008. The diagnosis of dementia was made according to the Diagnostic and Statistical Manual of Mental Disorders, Fourth Edition (DSM-IV) criteria (American Psychiatric Association, 1994). The diagnosis of Alzheimer's disease was made according to the National Institute of Neurological and Communicative Disorders and Stroke and the Alzheimer's Disease and Related Disorders Association (NINCDS–ADRDA) criteria (McKhann et al., 1984). Each patient received a uniform evaluation including a medical history, and physical and neurological examination. The Mini-Mental State Examination (MMSE) was used for the assessment of cognitive function. The BPSD were evaluated using the Neuropsychiatric Inventory (NPI) (Cummings et al., 1994). The Barthel Index, the higher scores of which indicate better performance, was used for the assessment for the ADL (Mahoney and Barthel, 1965). We included patients who satisfied the following criteria: (1) patients with AD at an age between 55 years and 85 years, (2) an MMSE score of ≥6 and ≤23 after the treatment with sulpiride 50 mg/day for 2 weeks, (3) presence of BPSD with a NPI score of ≥6 on at least 1 of the delusions, hallucinations, agitation/aggression, disinhibition, irritability/lability or aberrant motor activity subscales after the treatment with sulpiride 50 mg/day for 2 weeks, and (4) stable physical condition for at least the past year. The exclusion criteria were (1) treatment with Chinese herbal medicine other than YKS and psychotropic medication other than sulpiride, AchEI and anti-parkinsonism drugs, (2) other types of dementia, (3) delirium and amnesia due to drug use, metabolic intoxication or inflammation, (4) major physical illness such as neoplasma and acute inflammation that would likely prevent completion of the study. The Institutional Review Board of Kyushu University Hospital approved this study. All subjects gave informed consent according to the institutional guidelines and the recommendations of the Declaration of Helsinki.

2.2. Intervention and measurements

We included 15 patients who met the inclusion criteria in the present study. After a detailed explanation of the study, we obtained written informed consent from the participants and /or their families. At baseline, the MMSE and NPI were evaluated. All patients started to take sulpiride 50 mg/day. Sulpiride, which is a dopamine D_2 selective antipsychotic, is frequently used for the treatment of the BPSD in Japan although it is not a well-known antipsychotic outside Japan. After 2 weeks of sulpiride treatment (baseline), the MMSE, the NPI, and the Barthel Index were evaluated to select the patients with AD who did not favorably respond to sulpiride. According to the NPI scores at the baseline, 15 patients were included in the present study. These patients were randomly assigned to the YKS group ($N=10$) and the control group ($N=5$) using a random number table. The demographic data of the patients are shown in Table 1. One patient of the control group was excluded from the present study because of the emergence of severe peripheral edema. Ten patients of the YKS group received 2.5 g of YKS (1.5 g of extract) three times every day before meals for 12 weeks. All patients continued to take sulpiride 50 mg/day and were reassessed every 4 weeks by the NPI as well as the Barthel Index. The dose of sulpiride was changed according to the following criteria; (1) an NPI score of ≥8 on at least 1 of the delusions, hallucinations, agitation/aggression, disinhibition, irritability/lability or aberrant motor activity subscales resulted in an increase of the sulpiride dose of 50 mg/day (2) an NPI score of <4 on all of the above subscales: resulted in a decrease of the sulpiride dose of 50 mg/day. To examine the existence of adverse effects, we observed general conditions, including extrapyramidal signs and peripheral edema and hypokalemia. The laboratory data of all the patients were evaluated every 4 weeks.

2.3. Data analysis

The statistical assessment of the treatment effects on each study variable was performed using non-parametric statistics. In all of the analyses p-values <0.05 were considered to be significant. The data are presented as the mean±SD.

3. Results

After the 12 weeks of treatment with YKS, significant improvement of the mean NPI score was observed while no significant improvement was observed in the control group (Fig. 1). No significant improvement was observed in each subscale of the NPI. (data not shown) The average dose of sulpiride at the end of the present study tended to be less in the YKS group than in the control group ($p=0.141$). (Fig. 2). The MMSE results did not significantly change either in the

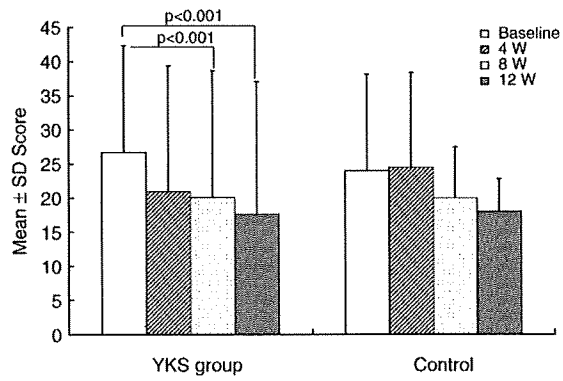

Fig. 1. The results of the neuropsychiatric inventory (NPI). After 12 weeks of treatment of YKS, significant improvement of the mean NPI score was observed while no significant improvement was observed in the control group. In all the analyses p-values <0.05 were considered to be significant. The data are presented as the mean±SD.

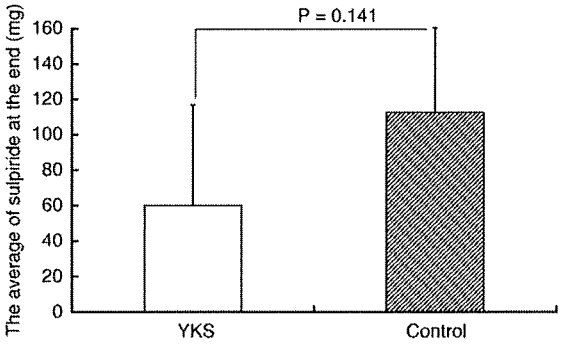

Fig. 2. The dose of sulpiride. The average dose of sulpiride at the end of the present study tended to be less in the YKS group than in the control group. (p=0.141) In all the analyses p-values <0.05 were considered to be significant. The data are presented as the mean±SD.

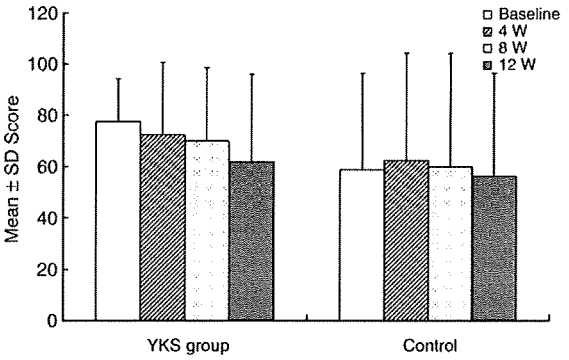

Fig. 4. The results of the Barthel Index. The Barthel Index did not significantly change either in the YKS group or in the control group. In all the analyses p-values <0.05 were considered to be significant. The data are presented as the mean±SD.

YKS group or in the control group (Fig. 3). The Barthel Index did not significantly change either in the YKS group or in the control group (Fig. 4).

Two patients of the YKS group showed hypokalemia possibly due to the YKS treatment and one of them was supplemented with potassium until the end of the study. Extrapyramidal signs were observed in 1 patient of the YKS group and the dose of sulpiride was reduced from 150 mg/day to 100 mg/day.

4. Discussion

To the best of our knowledge, there have been a few studies on the effect of YKS on BPSD. Iwasaki et al. reported in a randomized, observer-blinded, controlled trial that YKS was effective for improvement of BPSD and ADL in 27 patients with dementia such as AD, vascular dementia, AD with cerebrovascular disease, and dementia with Lewy bodies (DLB). They have also shown YKS to be effective for BPSD in 15 patients with DLB, which had been refractory to the treatment with a cholinesterase inhibitor (Iwasaki et al., 2005a,b). Shinno et al. have shown a beneficial effect of YKS for psychiatric symptoms and the sleep structure of dementia with BPSD (Shinno et al., 2007, 2008). In their studies which included two patients with AD and three patients with DLB, polysomnography (PSG) revealed increases in total sleep, sleep efficiency, stage 2 sleep, and decreases in the number of arousal and periodic movements. All of these studies included dementia other than AD and the duration of the YKS treatment was 4 weeks. In the present study, 12 weeks of the YKS treatment significantly improved BPSD of AD while the average dose of sulpiride at the end of the present study tended to be less in the YKS group than in the control group. The 12 weeks of the YKS treatment did not cause any cognitive decline or ADL decline and no serious adverse effects were noted.

BPSD occur in 50–90% of AD patients and an imbalance between the different neurotransmitters (acetylcholine, serotonin, dopamine, noradrenaline) is related to the pathophysiology of BPSD in AD (Lanari et al., 2006). YKS contains several herbal medicines (*Atractylodis Lanceae rhizona, Poria, Cnidii rhizoma, Angelicae Radix, Bupleuri Radix, Glycyrrhizae Radix* and *Uncariae Uncis Cum Ramulus*). Angelicae Radix, an important component of YKS, has been shown to affect γ-aminobutyric acid (GABA) and serotonin (5-HT) receptors (Liao et al., 1995). Growing evidence has suggested a role for 5-HT in BPSD. Postmortem studies have shown that cortical and subcortical 5-HT levels in AD patients with psychosis were lower than in patients without psychosis (Zubenko et al., 1991). Polymorphisms of the 5-HT_{2A} receptor (Assal et al., 2004; Lam et al., 2004) and the 5-HT transporter (Assal et al., 2004; Pritchard et al., 2007) have been reported to be related to the development of BPSD in AD. 5-HT_{2A} and 5-HT_{2C} polymorphisms have recently been reported to be relevant to BPSD of AD (Pritchard et al., 2008). Furthermore, it has also been reported that YKS inhibits the DOI (5-HT_{2A} and 5-HT_{2C} receptor agonist)-induced head-twitch response and decreases the expression of 5-HT_{2A} receptors in the prefrontal cortex of mice (Egashira et al., 2008). YKS has also been reported to enhance cholinergic transmission by a mechanism similar to that of AchEIs, which have been reported to be effective for the treatment of BPSD in AD (Lanari et al., 2006; Iwasaki et al., 2005a). Some of the ingredients of YKS also have affinity for dopamine receptors (Liao et al., 1995), and may particularly antagonize the dopamine D_2 receptor. These ingredients also have a sufficient affinity for 5-HT_2 receptors. Due to these pharmacological properties, extrapyramidal signs are rarely present even when YKS is prescribed to elderly patients (Iwasaki et al., 2005a). Furthermore, YKS has recently been reported to have an effect against beta amyloid-induced cytotoxicity on rat cortical neurons (Tateno et al., 2008). However, the present study included only a small number of populations and the heterogenous make up of the substance makes it difficult to propose a specific mechanism of action of YKS. Future studies which include larger patient populations, a longer duration of the YKS treatment, or the co-administration of AchEI and/or atypical antipsychotics with YKS should thus be performed. Further examinations using a double-blind placebo-controlled design should also be performed.

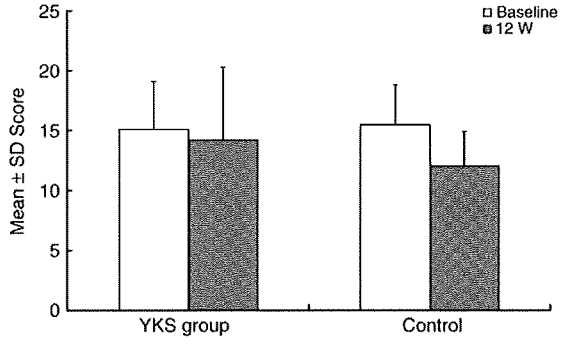

Fig. 3. The results of mini-mental state examinations (MMSE). MMSE results did not change either in the YKS group or in the control group. In all the analyses p-values <0.05 were considered to be significant. The data are presented as the mean±SD.

5. Conclusion

Twelve weeks of YKS treatment significantly improved BPSD with less antipsychotics in elderly patients with AD. The YKS treatment did not cause any cognitive decline or ADL decline and did not cause any serious adverse effects. The present study suggests that YKS is

beneficial for the treatment of BPSD and that it can possibly reduce the dose of antipsychotics required for the treatment of BPSD.

Acknowledgement

We acknowledge the financial support from TSUMURA & CO. (Tokyo, Japan) for the present study.

References

American Psychiatric Association. Diagnostic and Statistical Manual of Mental Disorders. 4th ed. Washington, DC: American Psychiatric Association; 1994.

Assal F, Alarcon M, Solomon EC, Masterman D, Geschwind DH, Cummings JL. Association of the serotonin transporter and receptor gene polymorphisms in neuropsychiatric symptoms in Alzheimer disease. Arch Neurol 2004;61(8):1249–53.

Cummings JL, Mega M, Gray K, Rosenberg-Thompson S, Carusi DA, Gornbein J. The Neuropsychiatric Inventory: comprehensive assessment of psychopathology in dementia. Neurology 1994;44(12):2308–14.

Dos Santos-Neto LL, de Vilhena Toledo MA, Medeiros-Souza P, de Souza GA. The use of herbal medicine in Alzheimer's disease—a systematic review. Evid Based Complement Alternat Med 2006;3(4):441–5.

Egashira N, Iwasaki K, Ishibashi A, Hayakawa K, Okuno R, Abe M, et al. Repeated administration of Yokukansan inhibits DOI-induced head-twitch response and decreases expression of 5-hydroxytryptamine $(5\text{-HT})_{2A}$ receptors in the prefrontal cortex. Prog Neuro-Psychopharmacol Biol Psychiatr 2008;32(6):1516–20.

Iwasaki K, Satoh-Nakagawa T, Maruyama M, Monma Y, Nemoto M, Tomita N, et al. A randomized, observer-blind, controlled trial of the traditional Chinese medicine Yi-Gan San for improvement of behavioral and psychological symptoms and activities of daily living in dementia patients. J Clin Psychiatr 2005a;66(2):248–52.

Iwasaki K, Maruyama M, Tomita N, Furukawa K, Nemoto M, Fujiwara H, et al. Effects of the traditional Chinese herbal medicine Yi-Gan San for cholinesterase inhibitor-resistant visual hallucinations and neuropsychiatric symptoms in patients with dementia with Lewy bodies. J Clin Psychiatr 2005b;66(12):1612–3.

Jeste DV, Blazer D, Casey D, Meeks T, Salzman C, Schneider L, et al. ACNP White Paper: update on use of antipsychotic drugs in elderly persons with dementia. Neuropsychopharmacology 2008;33(5):957–70.

Kuehn BM. FDA: Antipsychotics Risky for Elderly, 300 (4). JAMA; 2008. p. 379–80.

Lam LCW, Tang NLS, Ma SL, Zhang W, Chiu HFK. 5-HT_{2A}T102C receptor polymorphism and neuropsychiatric symptoms in Alzheimer's disease. Int J Geriat Psychiatr 2004;19(6):523–36.

Lanari A, Amenta F, Silvestrelli G, Tomassoni D, Parnetti L. Neurotransmitter deficits in behavioral and psychological symptoms of Alzheimer's disease. Mech Age Develop 2006;127(2):158–65.

Lawlor B. Managing behavioural and psychological symptoms in dementia. Br J Psychiatr 2002;181:463–5.

Liao JF, Jan YM, Huang SY, Wang HH, Yu LL, Chen CF. Evaluation with receptor binding assay on the water extracts of ten CNS-active Chinese herbal drugs. Proc Natl Sci Counc Repub China, B 1995;19(13):151–8.

Mahoney FI, Barthel DW. Functional evaluation:The Barthel Index. Md State Med J 1965;14:61–5.

McKhann G, Drachman D, Folstein M, Katzman R, Price D, Standlan EM. Clinical diagnosis of Alzheimer's disease: report of the NINCDS–ADRDA Work Group under the auspices of the Department of Health and Human Services Task Force on Alzheimer's Disease. Neurology 1984;34(7):939–44.

Mckeith I, Cummings J. Behavioural changes and psychological symptoms in dementia disorders. Lancet Neurol 2005;4(11):735–42.

Pritchard AL, Pritchard CW, Bentham P, Lendon CL. Role of serotonin transporter polymorphisms in the behavioural and psychological symptoms in probable Alzheimer disease patients. Dement Geriatr Cogn Disord 2007;24(3):201–6.

Pritchard AL, Harris J, Prichard CW, Coates J, Haque S, Holder R, et al. Role of 5HT2A and 5HT2C polymorphisms in behavioural and psychological symptoms of Alzheimer's disease. Neurobiol Aging 2008;29(3):341–7.

Rainer M, Haushofer M, Pfolz H, Struhal C, Wick W. Quetiapine versus risperidone in elderly patients with behavioural and psychological symptoms of dementia: Efficacy, safety and cognitive function. Eur Psychiatr 2007;22(6):395–403.

Shinno H, Utani E, Okazaki S, Kawamukai T, Yasuda H, Inagaki T, et al. Successful treatment with Yi-Gan San for psychosis and sleep disturbance in a patient with dementia with Lewy bodies. Prog Neuro-Psychopharmacol Biol Psychiatr 2007;31(7):1543–5.

Shinno H, Inami Y, Inagaki T, Nakamura Y, Horiguchi J. Effect of Yi-Gan-San on psychiatric symptoms and sleep structure at patients with behavioral and psychological symptoms of dementia. Prog Neuro-Psychopharmacol Biol Psychiatr 2008;32(3):881–5.

Schneider LS, Tariot PN, Dagerman KS, Davis SM, Hsiao JK, Ismail MS, et al. Effectiveness of atypical antipsychotic drugs in patients with Alzheimer's disease. N Engl J Med 2006;355(15):1525–38.

Sultzer DL, Davis SM, Tariot PN, Dagerman KS, Lebowitz BD, Lyketsos CG, Rosenheck RA, et al. Clinical symptom responses to atypical antipsychotic medications in Alzheimer's disease: Phase 1 outcomes from CATIE-AD effectiveness trial. Am J Psychiatr 2008;165(7):844–54.

Tateno M, Ukai W, Ono T, Saito S, Hashimoto E, Saito T. Neuroprotective effects of Yi-Gan San against beta amyloid-induced cytotoxicity on rat cortical neurons. Prog Neuro-Psychopharmacol Biol Psychiatr 2008;32:1704–7.

Zubenko GS, Moosy J, Martinez AJ, Rao G, Claassen D, Rosen J, et al. Neuropathologic and neurochemical correlates of psychosis in primary dementia. Arch Neurol 1991;48(6):619–24.

NEUROPATHOLOGY

Neuropathology 2009; **29**, 536–542 doi:10.1111/j.1440-1789.2009.01007.x

Original Article

Prion protein oligomers in Creutzfeldt-Jakob disease detected by gel-filtration centrifuge columns

Haruhiko Minaki, Kensuke Sasaki, Hiroyuki Honda, Toru Iwaki

Department of Neuropathology, Neurological Institute, Graduate School of Medical Sciences, Kyushu University, Fukuoka, Japan

Prion diseases are diagnosed by the detection of accumulation of abnormal prion protein (PrP) using immunohistochemistry or the detection of protease-resistant abnormal PrP (PrP^{res}). Although the abnormal PrP is neurotoxic by forming aggregates, recent studies suggest that the most infectious units are smaller than the amyloid fibrils. In the present study, we developed a simplified method by applying size-exclusion gel-filtration chromatography to examine PrP oligomers without proteinase K digestion in Creutzfeldt-Jakob disease (CJD) samples, and evaluated the correlation between disease severity and the polymerization degree of PrP. Brain homogenates of human CJD and non-CJD cases were applied to the gel-filtration spin columns, and fractionated PrP molecules in each fraction were detected by western blot. We observed that PrP oligomers could be detected by the simple gel-filtration method and distinctly separated from monomeric cellular PrP (PrP^{c}). PrP oligomers were increased according to the disease severity, accompanied by the depletion of PrP^{c}. The separated PrP oligomers were already protease-resistant in the case with short disease duration. In the cases with quite severe pathology the oligomeric PrP reached a plateau, which may indicate that PrP molecules could mostly develop into amyloid fibrils in the advanced stages. The increase of PrP oligomers correlated with the degree of histopathological changes such as spongiosis and gliosis. The decrease of monomeric PrP^{c} was unexpectedly obvious in the diseased cases. Dynamic changes of both oligomerization of the human PrP and depletion of normal PrP^{c} require further elucidation to develop a greater understanding of the pathogenesis of human prion diseases.

Key words: centrifugation, Creutzfeldt-Jakob disease, gel-filtration chromatography, oligomers, prion proteins.

INTRODUCTION

Prion diseases or transmissible spongiform encephalopathies (TSEs) are a group of fatal neurodegenerative disorders which include scrapie and bovine spongiform encephalopathy (BSE) in animals, and Creutzfeldt-Jakob disease (CJD) in humans. Histopathological changes of the brain are comprised of fine vacuolation, also termed spongiosis, reactive changes of astrocytes, and variable loss of neurons.[1] TSEs are associated with abnormal deposition of prion protein (PrP). The normal, cellular PrP (PrP^{c}) is converted into abnormal PrP (PrP^{sc}) through a process of conformational change where a portion of its α-helical and coil structure is refolded into a β-sheet.[2] PrP^{c} consists of 254 amino acids, and is attached to the cell membrane via a glycosyl-phosphatidylinositol anchor, a membrane glycoprotein expressed in many normal tissues and at higher levels in the brain.[2]

Under physiological conditions, PrP exists as 32–35 kDa protein.[3] PrP^{c} is soluble in detergent and degraded easily by proteases. By contrast, PrP^{sc} is insoluble in detergent and partially resistant to proteases.[3] The method for measurement of PrP^{sc} was fundamentally changed with the development of the conformation-dependent immunoassay (CDI). The CDI uses anti-PrP antibodies that react with an epitope exposed in native PrP^{c}, but which do not bind to native PrP^{sc}, which indicates the conformational change of PrP^{sc}. Studies using the CDI method have demonstrated that most PrP^{sc} is protease sensitive ($sPrP^{sc}$).[4–6] PrP^{sc}

Correspondence: Kensuke Sasaki, MD, Department of Neuropathology, Neurological Institute, Graduate School of Medical Sciences, Kyushu University, 3-1-1 Maidashi, Higashi-ku, Fukuoka 812-8582, Japan. Email: ksasaki@np.med.kyushu-u.ac.jp

Received 17 December 2008; revised 6 January 2009 and accepted 7 January 2009; published online 5 March 2009.

produces neurotoxicity by forming aggregates, and the most infectious units are much smaller than the amyloid fibrils that are often observed in TSE-infected tissues.[7,8] In uninfected human brains, PrP is mainly present in monomeric, dimeric, trimeric, and tetrameric forms, while a small amount of large PrP aggregates are present.[9] By contrast, in prion-infected brains the levels of large PrP aggregates are dramatically increased, although the monomers and small oligomers are still detected.[9,10]

Accumulation of misfolded proteins as insoluble aggregates occurs in several neurodegenerative diseases including dementia with Lewy bodies (DLB),[11] Huntington's disease,[12] Parkinson's disease (PD),[11,12] and Alzheimer's disease (AD),[12–14] and are associated with the formation and accumulation of amyloid fibrils in specific brain areas. In these fibrils and aggregates, the constituent molecules are largely in the β-conformation.[11] Recent studies suggest that the soluble oligomers may be the principal neurotoxic agents. Soluble Aβ oligomers are found in CSF of AD patients; the soluble Aβ content of the human brain is better correlated with the severity of disease than the classical amyloid plaques containing insoluble Aβ deposits,[13] and fibril-free oligomers are toxic to cultured cells and neurons.[15–17] In DLB and PD, α-synuclein accumulates in insoluble inclusions; however, α-synuclein promotes the formation of highly soluble oligomers that precede the insoluble α-synuclein aggregates associated with neurodegeneration.[11]

Prion diseases are conventionally diagnosed by the detection of accumulation of abnormal PrP using immunohistochemistry or the detection of the abnormal PrP with protease resistance (PrP^{res}). Comparison between CDI and western blotting of brain samples from sporadic CJD and variant CJD patients showed that the CDI was 50- to 100-fold more sensitive.[6] It would be highly recommended that the abnormality of PrP molecules should be determined from various perspectives more than protease resistance. In the present study, we tested several spin columns to detect PrP oligomers by a simplified method applying gel filtration chromatography without protease treatment, in CJD patients with various degree of neuropathological change, and evaluated the correlation between the disease severity and the degree of PrP polymerization.

MATERIALS AND METHODS

Brain homogenate preparation

Human brains were collected at autopsy from six sporadic CJD (methionine homozygote at the polymorphic codon 129 and the type 1 PrP^{res}: MM1; one case had an unknown genotype due to the refusal of genetic analyses) and three non-CJD neurological control cases (Table 1). The speci-

Table 1 Details of samples and the grading scores of spongiosis and gliosis

Case no.	Diagnosis	codon129/ PrP^{res} type	Age	Gender	Postmortem time (hours)	Duration of illness (months)	Brain weight (g)	Grading		Oligomer ratio	Monomer ratio
								Spongiosis	Gliosis		
1	sCJD	NA/type1	66	M	NA	2.5	1435	1	1	0.0563	0.1948
2	sCJD	MM/type1	68	F	12.5	2	1260	2	1	0.2606	0.2336
3	sCJD	MM/type1	73	F	19.5	4	1100	3	2	0.473	0.0623
4	sCJD	MM/type1	69	M	8	15	940	4	3	1.1263	0.046
5	sCJD	MM/type1	61	M	3.5	30	745	4	3	0.8908	0.0459
6	sCJD	MM/type1	71	M	NA	10	562	4	3	1.0854	0.069
7	Depression		47	M	4	NA	1490			0.0214	0.8418
8	ALS		68	M	5.5	NA	1470			0.02	0.4787
9	MG		59	M	2	NA	1350			0.0414	0.6879

sCJD, sprodaic CJD; ALS, amyotrophic lateral sclerosis; F, female; M, male; MG, myasthenia gravis; MM, methionine homozygote at prion protein gene codon129 polymorphism; NA, not available/applicable.

mens were stored at −80°C until used. Brain samples of frontal cortex were homogenized to a final concentration of 10% (w/v) in lysis buffer without sodium dodecyl sulfate (SDS) (100 mmol Tris-HCl, 100 mmol NaCl, 10 mmol EDTA, 0.5% Nonidet P-40 (NP-40), 0.5% deoxycholate, pH 7.6)[18] or in lysis buffer with SDS (100 mmol Tris-HCl, 100 mmol NaCl, 10 mmol EDTA, 1% SDS, pH 7.6). Samples were homogenized at 5000 rpm for 30 s in a bead-disrupter homogenizing system (MicroSmash MS-100; Tomy Seiko Co., Ltd., Tokyo, Japan). Homogenates were then clarified by centrifugation at 250 *g* for 5 min and the supernatant was stored at −80°C.

Spin-column gel filtration

The manufacturer's instructions for the columns (BD CHROMA SPIN™-200, 400; Clontech, San Francisco, CA, USA) indicated that the CHROMA SPIN-200 was capable of retrieving nucleic acids more than 350 bases and eliminating proteins smaller than 1000 kDa. The columns were pretreated by centrifuging at 200 *g* for 3 min to discard the storage buffer, and then 500 μL lysis buffer was added and centrifuged at 200 *g* for 3 min twice for the buffer exchange. To determine the protein shift, 0.01% bromophenol blue was added and 75 μL samples were then added to the center of the gel bed. The first centrifugation was made at 120 *g* for 2 min, and the first fraction was collected in the collection tube. Another 40 μL of lysis buffer was added, followed by centrifuging at 120 *g* for 2 min to collect the size-exclusion fractions sequentially. In these operations, we used a centrifuge with a fixed-angle rotor (RA-44; Kubota, Osaka, Japan) or swing-bucket rotor (A-4-62; Eppendorf, Hamburg, Germany). The centrifugal conditions described above were used for the swing-rotor centrifuge, and a milder centrifugation of 120 *g* to prepare the columns and 60 *g* to collect the fractions was used for the fixed angle rotor. Additionally, the fractions and pre-column brain homogenates were treated with 50 μg/mL proteinase-K (PK) to verify whether they contained PrP^{res}.

To evaluate the fractionation profiles we applied western protein standards (MagicMark XP; Invitrogen, Carlsbad, CA, USA) to a spin column. Marker proteins were prepared in sample buffer (NuPAGE LDS sample buffer; Invitrogen) and fractionated by the spin-column gel filtration method. Each fraction was assessed by western blot analysis.

Detection of fractionated prion proteins

Fractionated samples were boiled for 10 min in NuPAGE LDS sample buffer. Proteins were separated by SDS-polyacrylamide gel electrophoresis (SDS-PAGE) in 12% Bis-Tris gels (Invitrogen), and proteins were transferred to polyvinylidene difluoride (PVDF) membranes (Immobilon-P; Millipore, Billerica, MA, USA). The membranes were incubated for 1 h at room temperature with EzBlock (ATTO, Tokyo, Japan) in Tris buffered saline with Tween-20 (TTBS) (10 mmol Tris-HCl, 150 mmol NaCl, 0.05% Tween-20) to block the nonspecific binding of antibodies. Membranes were then incubated for 1 h at room temperature with an anti-prion antibody (mouse monoclonal 3F4, 1:10 000; Signet, Dedham, MA, USA), followed by a peroxidase-conjugated anti-mouse IgG secondary antibody (AP192P, 1:20 000; Chemicon, Temecula, CA, USA). Immunoreaction was visualized using ECL plus Western Blotting Detection System (GE Healthcare; Chalfont St. Giles, Buckinghamshire, UK).

Histopathological grading

The spongiform change and gliosis in the frontal cortex adjacent to the sampling site for brain homogenate preparation for each case were evaluated with HE staining and GFAP immunostaining. The grading criteria of the spongiosis were: 0, none; 1, mild (scattered or focal state); 2, moderate (patchy or laminar state); 3, severe (spread to the whole cortex); and 4, (rarefaction, i.e. status spongiosus). The grading criteria of the gliosis were: 0, none; 1, mild (slightly increased number of astrocytes); 2, moderate (prominent astrocytic cell processes); and 3, severe (numerous hypertrophic astrocytes).

RESULTS

Results from the fractionated molecular weight marker suggested that fractions two to four contained protein molecules of at least 220 kDa or more (Fig. 1). Fraction one consisted mostly of void volume, and was thus unsuitable

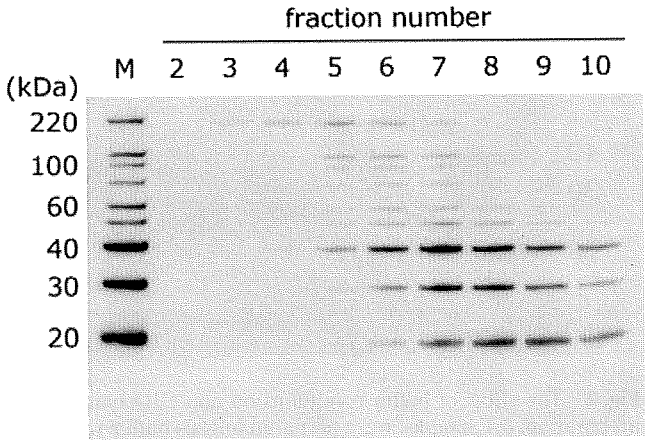

Fig. 1 Western blot analysis for the fractionated molecular markers (MagicMark XP, lane M). Fractions two to four consisted of molecules greater than 220 kDa. Fractions six to nine consisted of molecules of 20–40 kDa.

for assessment. It is estimated that monomeric PrP (size approximately 32–35 kDa) should be mainly collected in fractions six to eight. The experiment with the fixed-angle centrifuge showed a similar fraction pattern as that with the swing-bucket rotor (data not shown).

Proteins were not well separated by CHROMA SPIN-400, which had a pore size larger than CHROMA SPIN-200, particularly in the late-phase fractions (data not shown). Potentially, the gels with the large pores may be too tender to maintain their filtration capacity under the centrifugal conditions used in the present study. Some non-CJD homogenates in the lysis buffer with 0.5% NP-40 and 0.5% deoxycholate showed insoluble PrP aggregates in the peak fractions four to six (Fig. 2a). Therefore, we added 1% SDS in lysis buffer so that most of the PrP molecules were solubilized and detected in fractions six to eight (Fig. 2b). In human CJD brain homogenates, PrP was mostly detected in fractions two to four in an aggregated form (Fig. 3d,i). By contrast, PrP molecules in non-CJD brain samples were detected in fractions six to eight in a monomeric form (Fig. 2b).

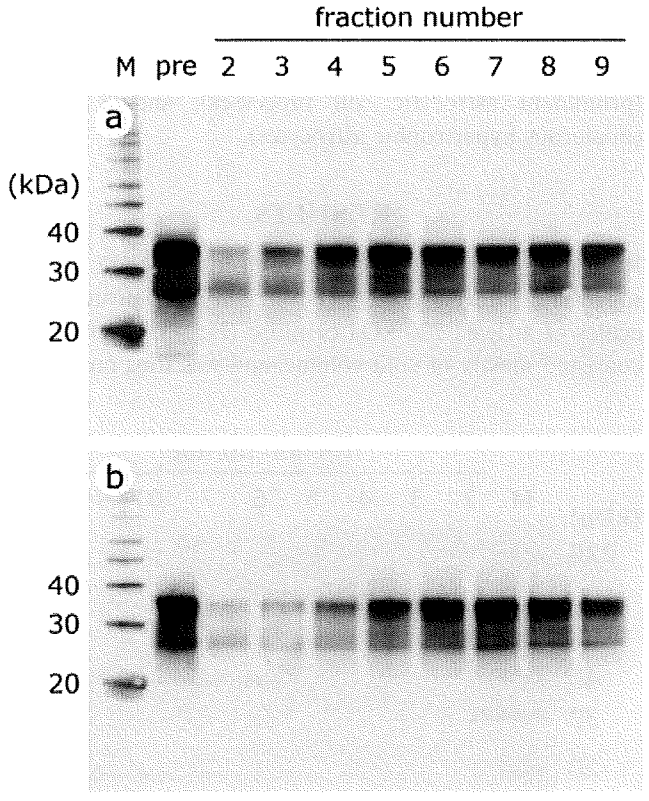

Fig. 2 The effect of buffer conditions on non-CJD homogenate preparation. (a) Samples were prepared in lysis buffer with 0.5% NP-40 and 0.5% deoxycholate, resulting in the detection of PrP molecules in the peak fractions four to six. (b) Most of the PrP molecules were solubilized in the lysis buffer with 1% SDS and shifted into fractions six to eight. pre: Pre-column brain homogenate.

The comparisons of histopathological features between the cases can be seen in Table 1. The findings in the representative cases with short and long disease duration (case 2 and case 5, respectively) can be seen in Figure 3. HE staining (Fig. 3a,f) and GFAP immunostaining (Fig. 3c,h) revealed that spongiosis and gliosis were advanced according to loss of brain weight. All of the CJD cases showed varying degrees of synaptic PrP deposition by PrP immunostaining (Fig. 3b,g). In the case with mild pathological change, PrP molecules were detected as aggregates in fractions two to four, and also as monomers in fractions six to eight (Fig. 3d), whereas in the severe case most of the PrP molecules were aggregated and detected in fractions two to four (Fig. 3i). PrP oligomers retrieved using this method had already developed PK resistance in both the mild and the severe cases (Fig. 3e,j).

The ratio of oligomeric/total PrP was increased according to the disease severity (Fig. 4). PrP oligomers were increased in inverse proportion to the brain weight; however, the ratio plateaued in the very severe cases (cases 1 and 2; Table 1). The increase of PrP oligomers correlated with the grade of histopathological change such as spongiosis and gliosis (Table 1). Moreover, monomeric PrP molecules were consistently decreased in the CJD cases (Fig. 4). The cut-off value of the oligomer ratio was approximately 0.05 between CJD and non-CJD cases.

DISCUSSION

The main difference between the spin-column gel filtration method used in the present study and conventional methods such as western blotting or ELISA is the removal of the protease treatment step. Without protease treatment, protease-sensitive PrP in samples should be retained, and we demonstrated that the PrP molecules can be separated by gel-filtration centrifuge columns using a suitable gel size. The elution curve of each protein was rather broad due to the low resolution of the column; however, the fractionation pattern appeared to be sufficiently effective to distinguish abnormally aggregated PrP oligomers from monomeric PrP^{c} by their size. Fractions two to four contained PrP oligomers of more than 220 kDa, which were discriminated from the monomeric PrP molecules mostly eluted in fractions six to eight. Furthermore, the procedure is safe as the gel filtration method can be performed in a closed system. The CDI method also detects PK-sensitive PrP^{sc} without protease treatment; however this is not based on the polymerization degrees but on the conformational changes of PrP. Therefore, both the gel-filtration method and the CDI method have the advantage of being able to determine PrP^{sc} from different perspectives.

PrP oligomers were increased according to the disease severity in the CJD cases, accompanied by the depletion of

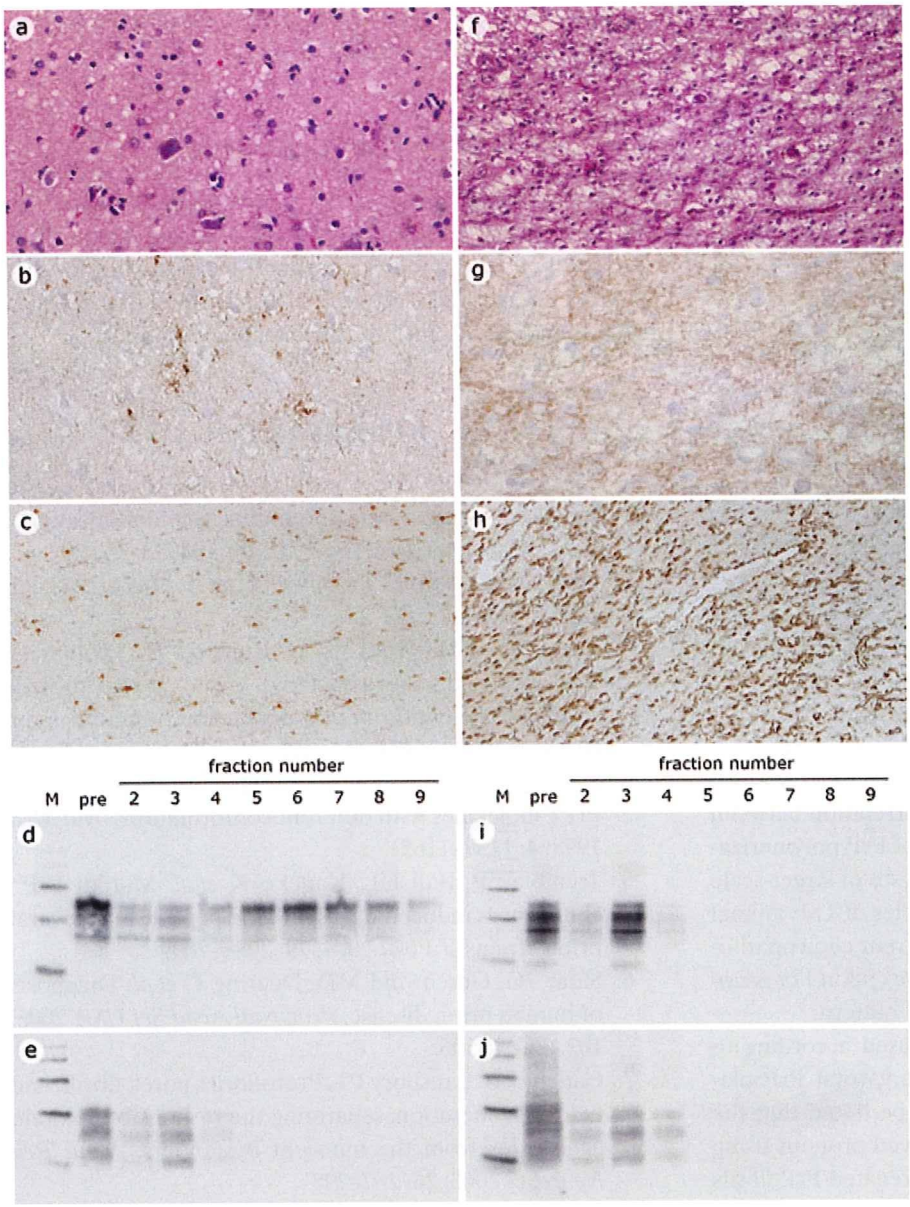

Fig. 3 Comparison of histopathological changes and fractionation patterns of PrP in the CJD cases with short disease duration (case 2 in Table 1, a–e) and long disease duration (case 5, f–i). (a, f) HE staining. (b, g) Immunostaining for PrP. (c, h) GFAP immunostaining. (d, i) Fractionation pattern for PrP. (e, j) Western blot for proteinase-K treated PrP in each fraction. pre: Pre-column brain homogenate. Objective magnification: ×20 (a, f), ×40 (b, g), and ×10 (c, h).

PrP^c. In the cases with short disease duration, CJD-specific pathological changes such as spongiform change, gliosis, and abnormal PrP deposition were less severely observed. PrP oligomers were detected in fractions two to four in those cases, whereas monomeric PrP^c was diminished compared to non-CJD control cases but were still detected in the brain. By contrast, PrP oligomers were more prominent in association with distinctly decreased PrP^c in the cases with long disease duration showing severe rarefaction (status spongiosus) and gliosis in the cerebral cortices. Since human autopsy samples of prion diseases would not exactly correlate with the progression of the disease, a time-course investigation could only be performed using serially collected samples of TSE animal models. However, the relationship of the polymerization degree of PrP to pathological severity such as loss of brain weight, spongiosis and gliosis indicates that dynamic changes of both oligomerization of the human PrP and depletion of normal PrP^c could be responsible for the pathogenesis of human prion diseases.

Previous reports on the polymerization degree of PrP determined by sucrose gradient sedimentation reveal that the PrP monomers and small oligomers are still detected in sporadic CJD samples[9] and prion-infected mouse brains.[10] In this study we demonstrated the almost total depletion of monomeric PrP in some cases with severe pathological changes, which may be due to more intense life-sustaining treatment in our cases. Furthermore, biochemical analyses on animal models would mostly be performed by means of whole brain materials including relatively intact regions,

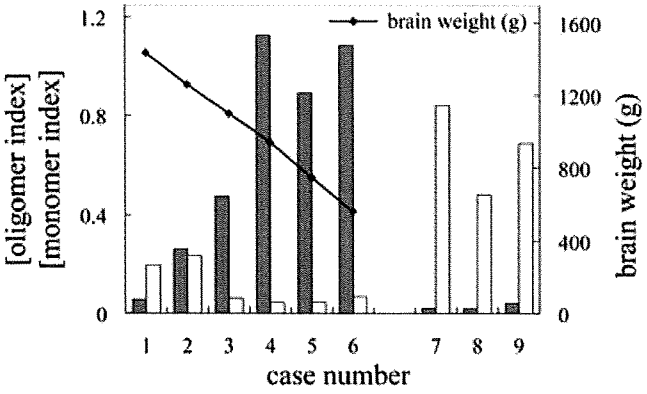

Fig. 4 Correlation between the oligomeric/monomeric PrP and brain weight. Fraction three in this method was supposed to represent the oligomeric PrP and fraction seven corresponded to the monomeric PrP. Pre-column samples were assumed as loading controls of total PrP. The density of triplet PrP bands in each lane was measured, and the oligomeric/total PrP or monomeric/total PrP was calculated as [oligomer index] (gray bars) or [monomer index] (open bars), respectively. The line graph shows the brain weight of CJD cases. The left y-axis shows the index of PrP and the right y-axis shows the brain weight (g).

whereas our biological data in this study were derived exclusively from the relevant lesions. Correlation between the disease progression and the degree of PrP polymerization requires further elucidation by analyses of larger-scale samples including serially collected samples of TSE animal models and human TSE cases with different clinicopathological features such as prion protein gene codon 129 genotypes, PrP^{sc} isoforms and PrP deposition pattern.

Although PrP oligomers were increased according to the disease stages, the ratio of oligomeric/total PrP plateaued in the very severe case. It must be noted that the uppermost limit of the size of the retrieved proteins using this method is unknown, and highly aggregated PrP fibrils may remain stuck in the gel bed. It is possible that abnormal PrP molecules would mostly form amyloid fibrils with a long disease duration, which could not be retrieved using this method. Sucrose gradient sedimentation was previously shown to detect all the detergent-insoluble PrP aggregates,[9,10] including amyloid fibrils, but the gel-filtration column method used in the present study is a suitable and more convenient method for retrieval of PrP oligomers.

In conclusion, the simplified gel-filtration method can detect PrP oligomers in human CJD cases. This method would detect not only PK-resistant PrP^{res}, but also PK-sensitive PrP^{sc}. The increase of PrP oligomers correlated with the degree of brain pathology such as spongiosis and gliosis. Further studies are required to confirm the biochemical characteristics of these oligomers, including the measurement of polymerization degree of PrP detected in fractions two to four, and whether these fractions are neurotoxic and/or infectious.

ACKNOWLEDGMENTS

This work was supported by grants to K. Sasaki from the Ministry of Health, Labour and Welfare, Japan (H19-nanchi-ippan-006) and the Japan Society for the Promotion of Science (No. 19500309). The authors thank Ms. S. Nagae and Ms. K. Sato for their technical support.

REFERENCES

1. Creutzfeldt HG. On a particular focal disease of the central nervous system (preliminary communication), 1920. *Alzheimer Dis Assoc Disord* 1989; **3**: 3–25.
2. Prusiner SB. Prions. *Proc Natl Acad Sci USA* 1998; **95**: 13363–13383.
3. Thackray AM, Hopkins L, Bujdoso R. Proteinase K-sensitive disease-associated ovine prion protein revealed by conformation-dependent immunoassay. *Biochem J* 2007; **401**: 475–483.
4. Safar J, Wille H, Itri V *et al.* Eight prion strains have PrP^{Sc} molecules with different conformations. *Nat Med* 1998; **4**: 1157–1165.
5. Tremblay P, Ball HL, Kaneko K *et al.* Mutant PrP^{Sc} conformers induced by a synthetic peptide and several prion strains. *J Virol* 2004; **78**: 2088–2099.
6. Safar JG, Geschwind MD, Deering C *et al.* Diagnosis of human prion disease. *Proc Natl Acad Sci USA* 2005; **102**: 3501–3506.
7. Caughey B, Lansbury PT. Protofibrils, pores, fibrils, and neurodegeneration: separating the responsible protein aggregates from the innocent bystanders. *Annu Rev Neurosci* 2003; **26**: 267–298.
8. Silveira JR, Raymond GJ, Hughson AG *et al.* The most infectious prion protein particles. *Nature* 2005; **437**: 257–261.
9. Yuan J, Xiao X, McGeehan J *et al.* Insoluble aggregates and protease-resistant conformers of prion protein in uninfected human brains. *J Biol Chem* 2006; **281**: 34848–34858.
10. Pan T, Wong P, Chang B *et al.* Biochemical fingerprints of prion infection: accumulations of aberrant full-length and N-terminally truncated PrP species are common features in mouse prion disease. *J Virol* 2005; **79**: 934–943.
11. Sharon R, Bar-Joseph I, Frosch MP, Walsh DM, Hamilton JA, Selkoe DJ. The formation of highly soluble oligomers of α-synuclein is regulated by fatty acids and enhanced in Parkinson's disease. *Neuron* 2003; **37**: 583–595.

12. Singer SJ, Dewji NN. Evidence that Perutz's double-β-stranded subunit structure for β-amyloids also applies to their channel-forming structures in membranes. *Proc Natl Acad Sci USA* 2006; **103**: 1546–1550.
13. Lue LF, Kuo YM, Roher AE *et al.* Soluble amyloid β peptide concentration as a predictor of synaptic change in Alzheimer's disease. *Am J Pathol* 1999; **155**: 853–862.
14. Walsh DM, Klyubin I, Fadeeva JV, Rowan MJ, Selkoe DJ. Amyloid-β oligomers: their production, toxicity and therapeutic inhibition. *Biochem Soc Trans* 2002; **30**: 552–557.
15. Dahlgren KN, Manelli AM, Stine WB *et al.* Oligomeric and fibrillar species of amyloid-β peptides differentially affect neuronal viability. *J Biol Chem* 2002; **277**: 32046–32053.
16. Kayed R, Head E, Thompson JL *et al.* Common structure of soluble amyloid oligomers implies common mechanism of pathogenesis. *Science* 2003; **300**: 486–489.
17. Lambert MP, Barlow AK, Chromy BA *et al.* Diffusible, nonfibrillar ligands derived from Aβ1-42 are potent central nervous system neurotoxins. *Proc Natl Acad Sci USA* 1998; **95**: 6448–6453.
18. Notari S, Capellari S, Giese A *et al.* Effects of different experimental conditions on the PrP^{Sc} core generated by protease digestion: implications for strain typing and molecular classification of CJD. *J Biol Chem* 2004; **279**: 16797–16804.